Functional classification of metabolic networks

Jorge Reyes

Program in Computational and Systems Biology,
Massachusetts Institute of Technology, Cambridge, MA 02139

Jörn Dunkel*

Department of Mathematics, Massachusetts Institute of Technology, Cambridge, MA 02139
(Dated: March 19, 2025)

Chemical reaction networks underpin biological and physical phenomena across scales, from microbial interactions to planetary atmosphere dynamics. Bacterial communities exhibit complex competitive interactions for resources, human organs and tissues demonstrate specialized biochemical functions, and planetary atmospheres are capable of displaying diverse organic and inorganic chemical processes. Despite their complexities, comparing these networks methodically remains a challenge due to the vast underlying degrees of freedom. In biological systems, comparative genomics has been pivotal in tracing evolutionary trajectories and classifying organisms via DNA sequences. However, purely genomic classifications often fail to capture functional roles within ecological systems. Metabolic changes driven by nutrient availability highlight the need for classification schemes that integrate metabolic information. Here we introduce and apply a computational framework for a classification scheme of organisms that compares matrix representations of chemical reaction networks using the Grassmann distance, corresponding to measuring distances between the fundamental subspaces of stoichiometric matrices. Applying this framework to human gut microbiome data confirms that metabolic distances are distinct from phylogenetic distances, underscoring the limitations of genetic information in metabolic classification. Importantly, our analysis of metabolic distances reveals functional groups of organisms enriched or depleted in specific metabolic processes and shows robustness to metabolically silent genetic perturbations. The generalizability of metabolic Grassmann distances is illustrated by application to chemical reaction networks in human tissue and planetary atmospheres, highlighting its potential for advancing functional comparisons across diverse chemical reaction systems.

Complex chemical reaction networks are central to the function of living and non-living systems across a wide range of length scales, from microscopic organisms [1–3] and tissues [4, 5] to ecosystems [6–8] and planetary atmospheres [9–11]. Recent advances in experimental and computational methods have enabled the comprehensive reconstruction of metabolic processes in various biological systems [12–15]. Similarly, the James Webb Space Telescope has produced high-quality spectroscopic data allowing the chemical characterization of exoplanet atmospheres in remarkable detail [16]. In bacterial communities, spatiotemporal pyruvate cross-feeding by swarming *Bacillus subtilis* has been observed; bacteria in the swarm front consume their preferred carbon source and deposit pyruvate which is consumed by bacteria in the bulk [17]. In mice and humans, models of metabolic processes have resolved metabolic cycles and energy use [5, 18, 19]. On the astrophysical scale, the topological distinctiveness of Earth's atmosphere,from the atmospheres of other celestial bodies in the Solar System, has suggested the development of network-based biosignatures [11]. In these examples, the breadth of chemistries is shaped by processes that are potentially inaccessible to perturbation or measurement, such as evolution, cellular differentiation, and atmospheric development. The vast number of underlying degrees of freedom presents a challenge to the formation of methodical and functional comparisons between chemical reaction networks.

In living systems, inferences of metabolic function from taxonomic classifications are inherently difficult; phylogenetically similar organisms may have vastly different metabolic capabilities [20–23]. In complex organisms, tissues and organs share the same genetic code and are yet capable of various metabolic functions [4]. Hence, functional roles cannot be readily ascribed to organisms with similar genetic and evolutionary backgrounds. To tackle this problem, we introduce here a conceptual and computational framework for comparing the topologies of various chemical reaction networks, by measuring distances between the nullspaces of their stoichiometric matrices [24–29].

Chemical reaction networks are naturally described by the mathematical theory of graphs in which chemical species are represented by vertices and physicochemical processes are represented by weighted and directed hyperedges which capture the direction and stoichiometric quantities of each process (Fig. 1) [26, 27]. Graphs of this flavor admit a matrix representation: the incidence or stoichiometric matrix S. Physically, these matrices
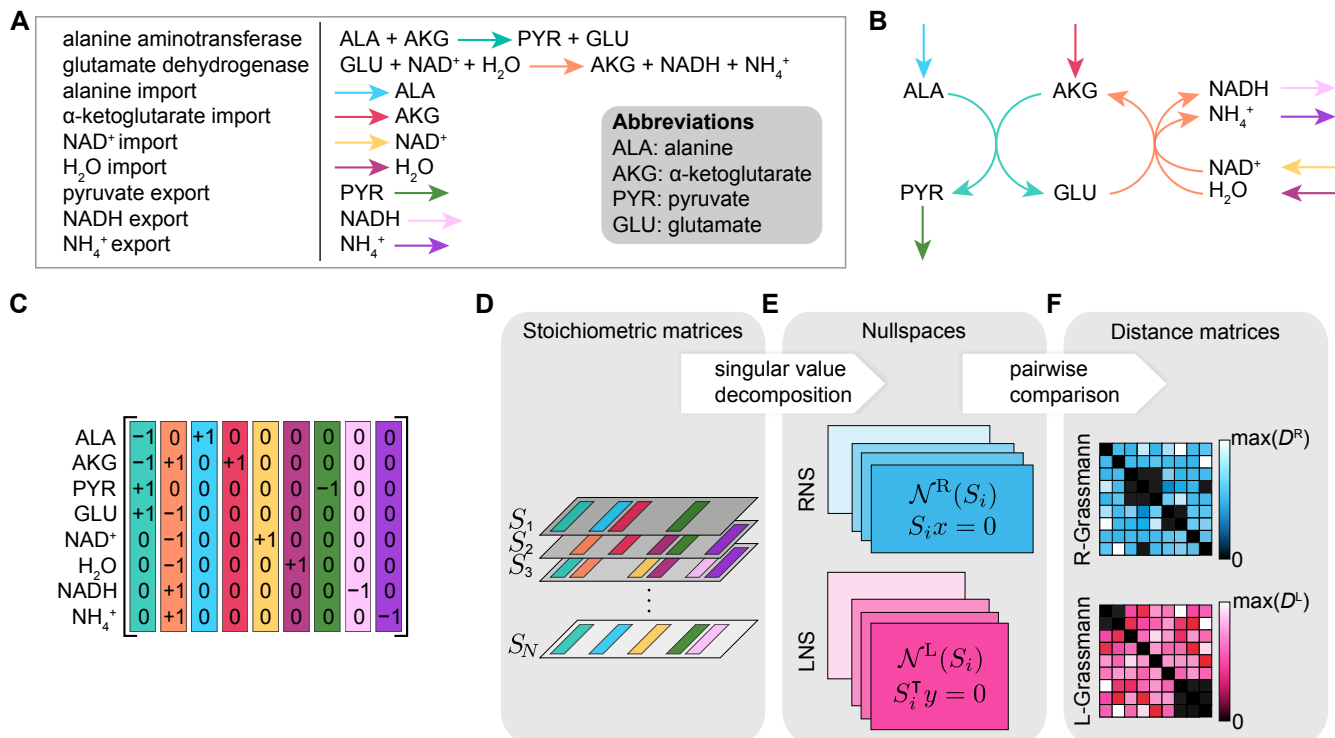
---
* dunkel@mit.edu

FIG. 1. **Metabolic Grassmann distances are calculated by comparing nullspaces of stoichiometric matrices.** Lists of chemical reactions and transport processes (A) are collected in graphs (B) where vertices and edges correspond to chemicals and processes, respectively. The tails and heads of an edge carry information about the number of chemicals consumed and produced by the process, accordingly. The graph representation in turn admits a matrix representation (C): the graph incidence or stoichiometric matrix whose entries are these weights up to a sign which captures whether a metabolite is consumed ($-$) or produced ($+$). (D) Row and column-sorted stoichiometric matrices are (E) transformed by computation of their right and left nullspaces—omitting rows and columns of full zeros which correspond to network-specific nonexistent metabolites and processes. (F) Networks are compared pairwise by applying the Grassmann distance metric (Eq. 2) to obtain a distance matrix. Abbr: RNS = right nullspace, LNS = left nullspace.

satisfy the mass-action kinetic differential equation:

$$\frac{\mathrm{d}c}{\mathrm{d}t} = Sv, \qquad (1)$$

where c is a vector of concentrations and v is a vector of fluxes. Each v_i corresponds to the net rate of change in concentrations of the chemical species involved in process i. Each v_i is a sum of directed fluxes: $v_i = v_i^{(+)} - v_i^{(-)}$ where directed fluxes are proportional to the probability of an encounter between reactants (or products) [28]. If the mathematical forms of these fluxes are known, the concentrations of chemicals in the network are readily obtained [30]. Without loss of generality, we will assume that all fluxes are reversible. Specifically, processes proceed in the forward direction if $v_i^{(+)} > v_i^{(-)}$, while for $v_i^{(+)} < v_i^{(-)}$ the process is reversed. The graph representation of chemical reaction networks makes distance metrics on graphs attractive choices. However, not all graph distance metrics are suitable for directed graphs with hyperedges; applications of these metrics typically ignore directionality or stoichiometry [31, 32]. Other existing metrics opt for computational tractability, such as re-

ducing the scope to comparisons of the presence/absence of metabolic processes [23, 33] or feature vectors of topological measures derived from a graph-theoretic approach [11, 34]. We avoid these information losses by leveraging advances in parallel computing and numerical linear algebra to make calculations of stoichiometric nullspaces tractable for large datasets [35, 36]. At this point, one may ask why focus on nullspaces of stoichiometric matrices?

Principally, the stoichiometric nullspaces have natural physical interpretations in terms of the mass-action picture of Eq. 1. The right nullspace of a stoichiometric matrix satisfies the nonequilibrium steady-state flux condition required by flux balance-based approaches [26, 27, 37], $Sv = 0$. Namely, the right nullspace contains linear combinations of processes that result in net zero consumption and production of all chemical species. This is equivalent to currents satisfying Kirchoff's current law in electrical circuits [28]. Contrast this with the left nullspace which consists of conservation laws for pools of chemicals [28, 38–41]. Indeed, we see that for an element

w of the left nullspace:

$$w \cdot \frac{\mathrm{d}c}{\mathrm{d}t} = w \cdot (Sv) = (S^{\mathsf{T}}w) \cdot v = 0 \implies w \cdot c = \text{constant}.$$

Previous characterizations of the left nullspace describe biological properties such as energy and redox potential, which are essential to meet energetic demands [38, 42–44]. The physical perspective offered by both nullspaces suggests that they are suitable candidates for developing a functional classification scheme of chemical reaction networks.

Distances between linear subspaces have already appeared in analyses of electroencephalogram signals [45],

network security [46] and undulatory worm locomotion [47]. The classic method of comparison uses that linear subspaces of dimension k embedded in $\mathbb{R}^n$ are elements of the Grassmannian manifold $\mathrm{Gr}(k, n)$ with a geodesic metric that is computed by singular value decomposition. This Grassmann distance metric generalizes in a nontrivial manner to linear subspaces of all dimensions, regardless of the value of k and n. The generalized Grassmann distance is defined on the manifold of linear subspaces of all dimensions, elements of the doubly infinite Grassmannian $\mathrm{Gr}(\infty, \infty)$. On $\mathrm{Gr}(\infty, \infty)$, the geodesic distance between subspaces with bases $A \in \mathrm{Gr}(k, \infty)$ and $B \in \mathrm{Gr}(\ell, \infty)$ is [29]:

$$d_{\mathrm{Gr}(\infty,\infty)}(A, B) = \left(|k - \ell| \, \pi^2/4 + \sum_{i=1}^{\min(k,\ell)} \theta_i^2 \right)^{1/2}, \quad \Theta = \mathrm{diag}(\theta_1, \ldots, \theta_{\min(k,\ell)}) = \cos^{-1} \Sigma \quad \text{where} \quad A^{\mathsf{T}}B = U\Sigma V^{\mathsf{T}}.$$

$$(2)$$

where the θ_i are the principal angles between the subspaces. If we consider $k \leq \ell$, the Grassmann distance metric provides a distance from the ℓ-dimensional subspace B to the furthest ℓ-dimensional subspace that contains the k-dimensional subspace A. The symmetric statement is also true: it is the distance from the k-dimensional subspace A to the furthest k-dimensional subspace contained in the ℓ-dimensional subspace B [29]. Herewithin, we will refer to the geodesic distance metric between right and left nullspaces, in the doubly infinite Grassmannian, as R-Grassmann and L-Grassmann, respectively.

We now move towards applications of the Grassmann distance to chemical reaction networks. First, we examine the effect of genetic perturbations in the genome of the model organism *Escherichia coli* K-12 MG1665 on these metabolic Grassmann distances [49]. We then consider genetically diverse organisms present in the AGORA2 (assembly of gut organisms through reconstruction and analysis, version 2) dataset which serves as a metabolic knowledge base for the human gut microbiome [49]. We show that the resulting Grassmann distances on nullspaces do not appreciably recapitulate taxonomic structures obtained from comparisons of the genetic background. To establish functional classifications, we identify metabolic process modalities that cluster organisms in each Grassmann distance, as well as the computationally tractable Jaccard distance [23, 33]. The final application of the Grassmann distance on the chemical reaction networks of human tissues [5] and planetary atmospheres [11] highlights the applicability of Grassmann distances to systems of different length scales and fields.

RESULTS

Robustness of metabolic Grassmann distances to genetic variations

To illustrate the robustness of the Grassmann distances to genetic perturbations in the form of gene knockouts (KO), we use the AGORA2 metabolic network of the model organism *E. coli* K-12 MG1655. We perform single gene deletions on the genome-scale network by evaluating gene-protein-reaction (GPR) rules that describe the mapping from gene presence to reaction presence [49]. This allows us to obtain 389 unique networks corresponding to these deletions where a specific network may correspond to many single gene KOs. Of these KOs, $\sim 82\%$ are computationally viable; they admit nonzero biomass flux in complete media with all possible external chemical inputs (SI). Furthermore, two-dimensional embeddings of the metabolic distance matrices, via stochastic gradient descent multidimensional scaling (sgd-MDS), demonstrate that the metrics considered here are capable of distinguishing computationally viable and unviable networks with the L-Grassmann distance attaining the best performance (SI).

We observe that most computationally viable single gene KOs lead to no or minimal changes in nullspaces (Fig. 2A *Top*). The exception observed here corresponds to $\Delta uidA$ that otherwise encodes for β-glucuronidase which, in the context of the human gut microbiome, modifies hydrophilic molecules for elimination by the host [50–52]. Previous work indicates that the *uidA* gene is nearly ubiquitous in *E. coli* isolates from treated and raw water sources [53].

To go beyond small genetic differences, let us focus on mini-AGORA2, a subset of the metabolic networks
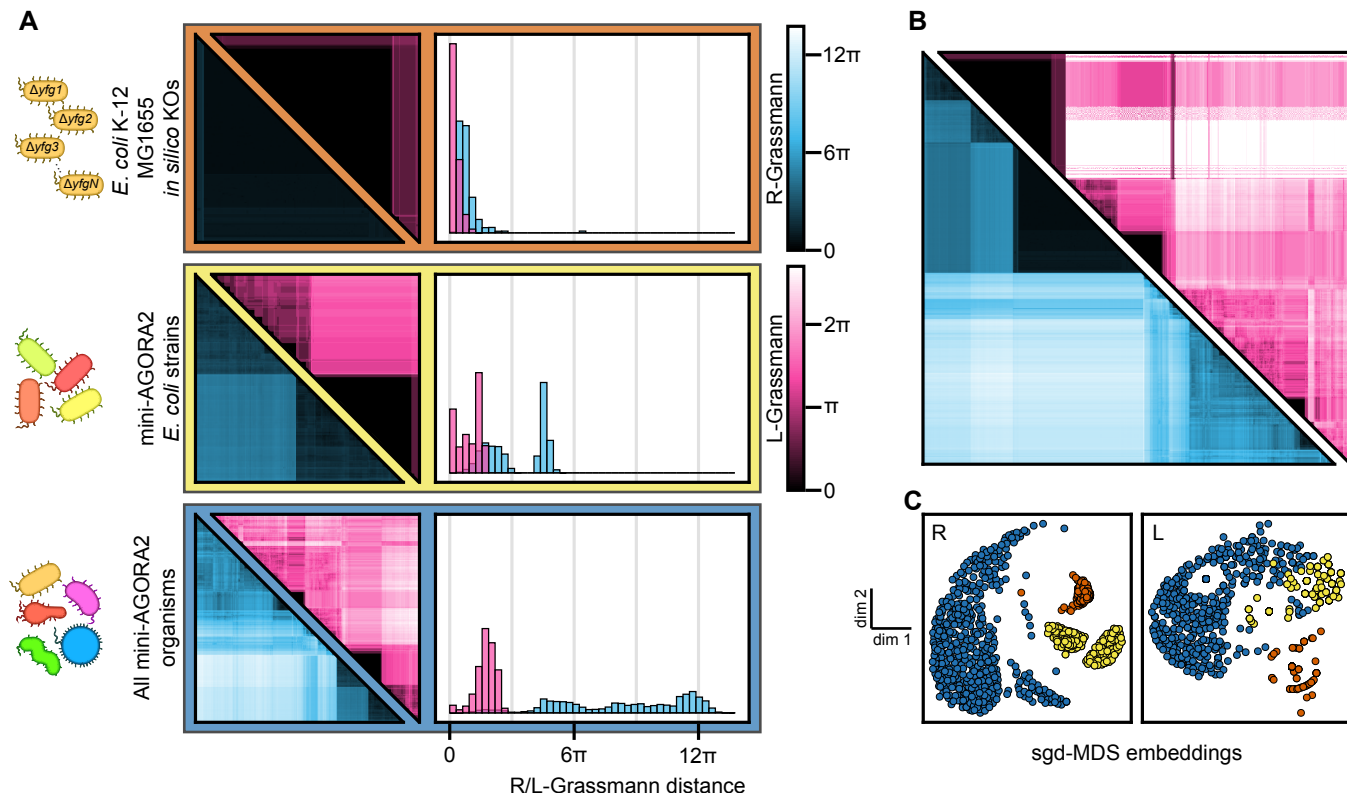
FIG. 2. **Metabolic Grassmann distances are robust to genetic perturbations and broaden with genetic diversity.** (*A*) Metabolic Grassmann distance matrices are computed for organisms at different scales of genetic similarity: computationally viable *Escherichia coli* K-12 MG1665 *in silico* KOs (top), *E. coli* strains in mini-AGORA2 (middle), and all mini-AGORA2 organisms along with distribution of these distances. Distance distributions show preferences for larger distances with increasing genetic diversity. (*B*) Joint distance matrix for all organisms considered in (*A*). (*C*) Stochastic-gradient descent multidimensional (sgd-MDS) embeddings are shown for all organisms considered in (A) with appropriate color schemes where blue corresponds to non-*E. coli* organisms in mini-AGORA2. All distance matrices are sorted by hierarchical clustering with Ward linkage. Bacteria images were obtained and modified from ref. 48 under a Creative Commons Attribution 4.0 International License.

of AGORA2, which represents 688 genetically distinct microbes [49]. With mini-AGORA2, we examine microbial metabolism as shaped by evolution and the human gut environment. We find that compared to the computationally viable KOs of *E. coli* K-12 MG1655, the mini-AGORA2 *E. coli* strains realize larger distances in both nullspaces (Fig. 2A *Middle*), which are further augmented when considering all mini-AGORA2 networks (Fig. 2 *Bottom*). Two-dimensional sgd-MDS embeddings of the combined Grassmann distance matrix (Fig. 2B) reveal that networks of viable *E. coli* KOs cluster away from the mini-AGORA2 networks (Fig. 2C). Note that this suggests that high genetic similarity may be sufficient to produce similar nullspaces.

Inequivalence of genetic and metabolic distances

To investigate the differences between Grassmann, Jaccard and genetic distances, we perform linear regression analyses with mini-AGORA2 distances for all pairs of

metrics. Here we take the genetic distance to be the square root of the tree distance on a phylogenetic tree which we infer from genome sequences using the PhyloPhlAn pipeline [54, 55]. We verify that small phylogenetic differences between two organisms can produce appreciable differences in nullspaces. Moreover, we find that the Grassmann distances display the least linear phylogenetic predictive power, unlike the Jaccard distance (Fig. 3). The latter is consistent with existing work that has shown an exponential relationship between the Jaccard distance and the cophenetic distance in human gut microbiome metabolic networks [23]. The cophenetic tree is an alternative genetic distance derived from phylogenetic trees that uses the height of the most recent common ancestor [56]. Together, these results suggest that the Jaccard distance is suboptimal for the purposes of forming metabolic classifications that go beyond phylogeny.

We compare each distance matrix by ordering the rows and columns by phylum for the five most abundant phyla in mini-AGORA2 metabolic networks. We
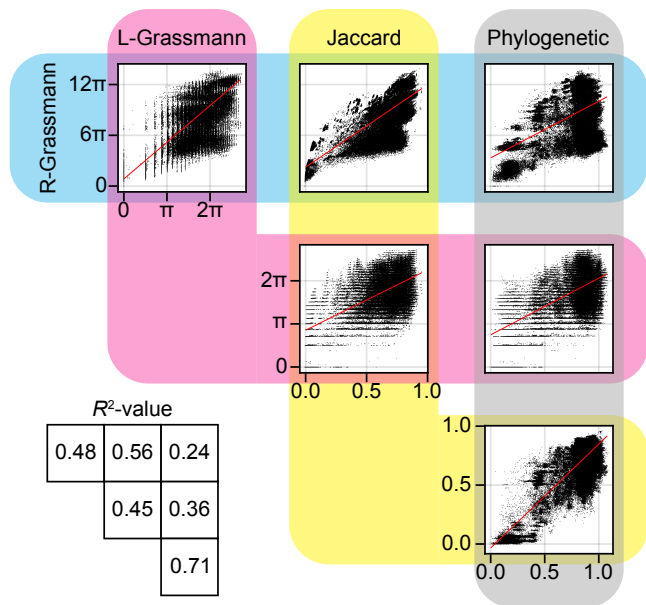
FIG. 3. **Inequivalence of metabolic and phylogenetic metrics in mini-AGORA2 organisms.** The Jaccard distances correlate the most with the phylogenetic distance which suggests that it is not the best choice for substantially distinguishing organisms beyond genetic differences. The line of best fit is shown in red with corresponding R^2-values on the bottom left. That the L-Grassmann distances appear quantized compared to the Jaccard metric suggest that metabolic network, despite having different metabolic processes, display similar conservation laws.

observe that this reordering produces a checkerboard-like pattern that loosely aligns with the phyla of the organisms (Fig. 4 *Top*). To validate goodness of clustering, we compute mean silhouette scores using phyla as cluster assignments. We find that the three metabolic distances produce values smaller than phylogenetic distance, indicating a loss of adherence to these categories. This is further illustrated by two-dimensional sgd-MDS embeddings (Fig. 4 *Bottom*).

Embedding and clustering highlights the phenotypic distinguishing power of metabolic distances

Metabolic processes are the smallest functional subunits of chemical reaction networks. As such, we seek to identify metabolic process modalities that lead to proximal nullspaces and opt for a cluster-based analysis, forgoing associating axes of low-dimensional embeddings to any particular aspect of metabolism. We use hierarchical clustering and tree-cuts with Ward's linkage to analyze eight clusters for each metabolic distance. In principle, any desired level of granularity can be considered using this approach. In the spirit of phylogenetic taxonomy [57, 58], we examine the coarser cases of 2 and 4 clusters (SI).

We identify metabolic processes whose presence or ab-

sence across networks closely matches binary inclusion in a given cluster using normalized variation of information (VI) [59] as a means of quantifying partition similarity. In this manner, we identify physicochemical processes that, when present or absent, entropically match cluster membership. Although single metabolic processes may be insufficient to fully explain differences in nullspaces, we find that different ckysters are enriched or depleted in different processes (Fig. 5). To understand the applicability of each metabolic distance, we focus on groups with VI that are less than 10% of the theoretical upper bound for binary partitions [59].

First, we note that ∼53% of the networks considered here are either *E. coli* KOs or strains which contribute to the presence of primarily *E. coli* clusters. Both Grassmann distances produce two clusters with the same process attributed to them: R-Grassmann groups 1 & 7 and L-Grassmann groups 1 & (weakly) 2. By comparison to Fig. 2, we find that both groups 1, which are enriched in trans-cinnamate exchange, correspond to almost all of the *E. coli* K-12 MG1655 KO, whereas the remaining groups, which are depleted in ATP:dUMP phosphotransferase, are primarily composed of *E. coli* and *Shigella flexneri* strains. Let us now consider clusters on a metric-specific basis.

R-Grassmann clustering identifies glucuronide-related processes

R-Grassmann groups 5 and 6 correspond to processes with glucuronidated chemicals. Glucuronide moieties are added to metabolic substrates to increase hydrophilicity to faciliate elimination from the human body. As a result, glucuronidation is critical for the removal of unwanted endogenous molecules, drugs, and xenobiotics [50–52]. Group 8, which is enriched in the pyrophosphate:oxaloacetate carboxy-lyase reaction, is entirely composed of *E. coli* strains. This reaction produces inorganic phosphate, carbon dioxide, and phosphoenolpyruvate from pyrophosphate (PP_i) and oxaloacetate. This process is analogous to the gluconeogeneic PECK reaction, which uses ATP instead of PP_i as a phosphate donor, but is unlikely to share an evolutionary origin [60–62].

L-Grassmann clusters match diverse metabolic processes

L-Grassmann group 5 lacks the CDP-diacylglycerol (n-C18:0) synthetase reaction which is involved in the production of a specific CDP-diacylglycerol from phosphatidic acid (18:0/18:0). In bacteria, CDP-diacylglycerols are precursors for the biosynthesis of all major phospholipids that comprise organelle membranes [60, 63]. Group 6 corresponds to organisms with the capacity for hydrogen sulfide (H_2S) oxidation which is notable since H_2S is known to be redox-active in the human gut [64]. In
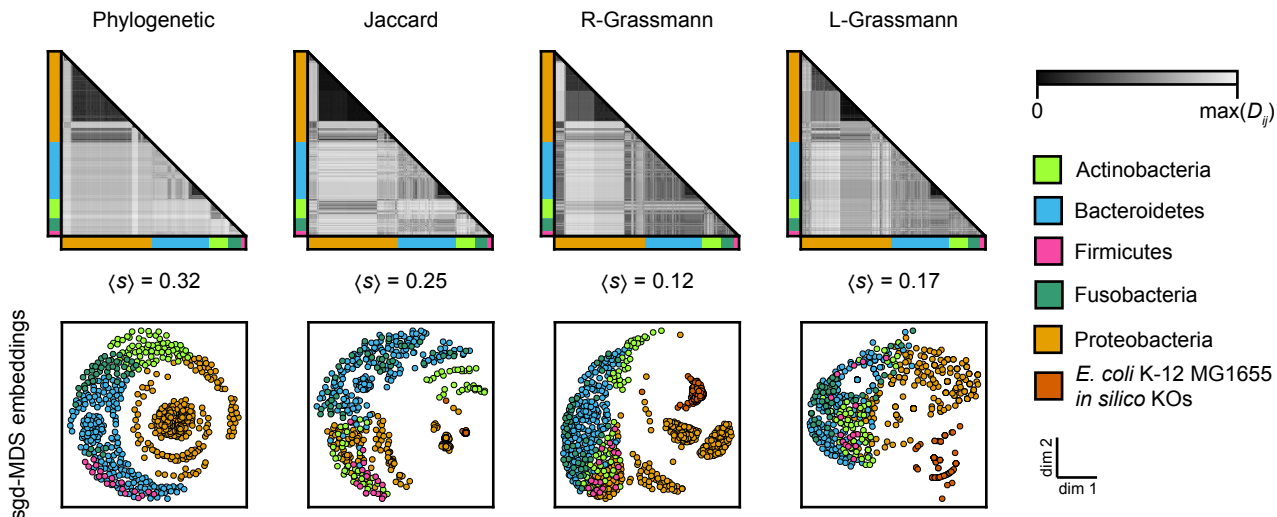
FIG. 4. **Euclidean embeddings of the metabolic distances suggest that organisms do not form distinct metabolic niches on the basis of phyla.** Mini-AGORA2 phylogenetic and metabolic distance matrices are sorted by organism phylum for the five most abundant phyla: Actinobacteria, Bacteroidetes, Firmicutes, Fusobacteria, and Proteobacteria. We exclude three other phyla each with one network. Mean silhouette scores $\langle s \rangle$ are computed for each distance using phyla as cluster assignments. Multidimensional scaling embeddings in $\mathbb{R}^2$ show loss of adherence to these phyla assignments across all metabolic distance when compared to the phylogenetic distance.

particular, recent work has shown that hydrogen sulfide drives the abiotic reduction of xenobiotics with azo moieties (R-N=N-R') [65]. Group 7 corresponds to organisms with 2-aminobut-2-enoate aminohydrolyase and L-methionine methanethiol-lyase reactions. These reactions constitute an L-methionine catabolic pathway in which methionine is broken down into methanethiol, α-ketobutryate and ammonia. Group 8 corresponds to organisms with the irreversible ADP-forming L-aspartate ammnonia ligase reaction. This reaction is responsible for producing L-asparagine by ADP-producing ammonia incorporation into L-aspartate [66]. Aspartate and asparagine are amino acids whose carbon skeletons originate from oxaloacetate, an intermediate of the citric acid cycle, and belong to a class of amino acids involved in nitrogen-fixation [60].

Jaccard distance

Jaccard group 1 corresponds to the presence of periplasmatic transport processes for metabolites conjugated to glucuronate, including the three most abundant estrogens—estradiol, estriol, and estrone—and the drug regorafenib [67]. Groups 3 and 4 correspond to transport processes via ATP-binding cassette (ABC) transporters that couple ATP hydrolysis to the influx and efflux of various substrates such as calcium and spermidine [68]. The Jaccard distance shares glucuornidation-related groups 7 and 8 with the R-Grassmann distance.

Grassmann distances on human tissue and planetary chemical reaction networks

The nullspace-based framework presented here is general and can be applied to complex chemical reaction networks on various length scales. As illustrative examples, we consider the chemical reaction networks of sex-specific human tissues [5] and planetary atmospheres [11].

Despite metabolic differences between tissues of different sexes, we find that the Grassmann distances group networks by tissue type (Fig. 6A). Moreover, we observe clustering based on hematopoietic-stem cell origin (B cells, CD4 T cells, monocytes, NK cells, platelets, and red blood cells) [69]. We observe that for the right nullspace, the kidneys, liver, colon, and brain remain distinguishable from most networks in a sgd-MDS embedding of the distance matrix, whereas for the left nullspace, we find that the pancreas, colon, lungs, and brain are the distal tissues (Fig. 6A). This highlights the tissue-specific diversity of steady-state fluxes and conservation laws.

To move towards chemical reaction networks on the astrophysical scale, we consider eight atmospheric networks corresponding to six celestial bodies (Fig. 6B). The networks used here are derived from a study on the chemical reaction networks of planetary atmospheres using graph topological measures [11]. With the exception of the "textbook" Earth model [10], these networks were obtained from published studies simulating the photochemistry of atmospheres using the photochemistry–transport model KINETICS from Caltech–JPL [9]. Importantly, we observe that the most distal network corresponds to the "textbook" Earth atmospheric model, which suggests
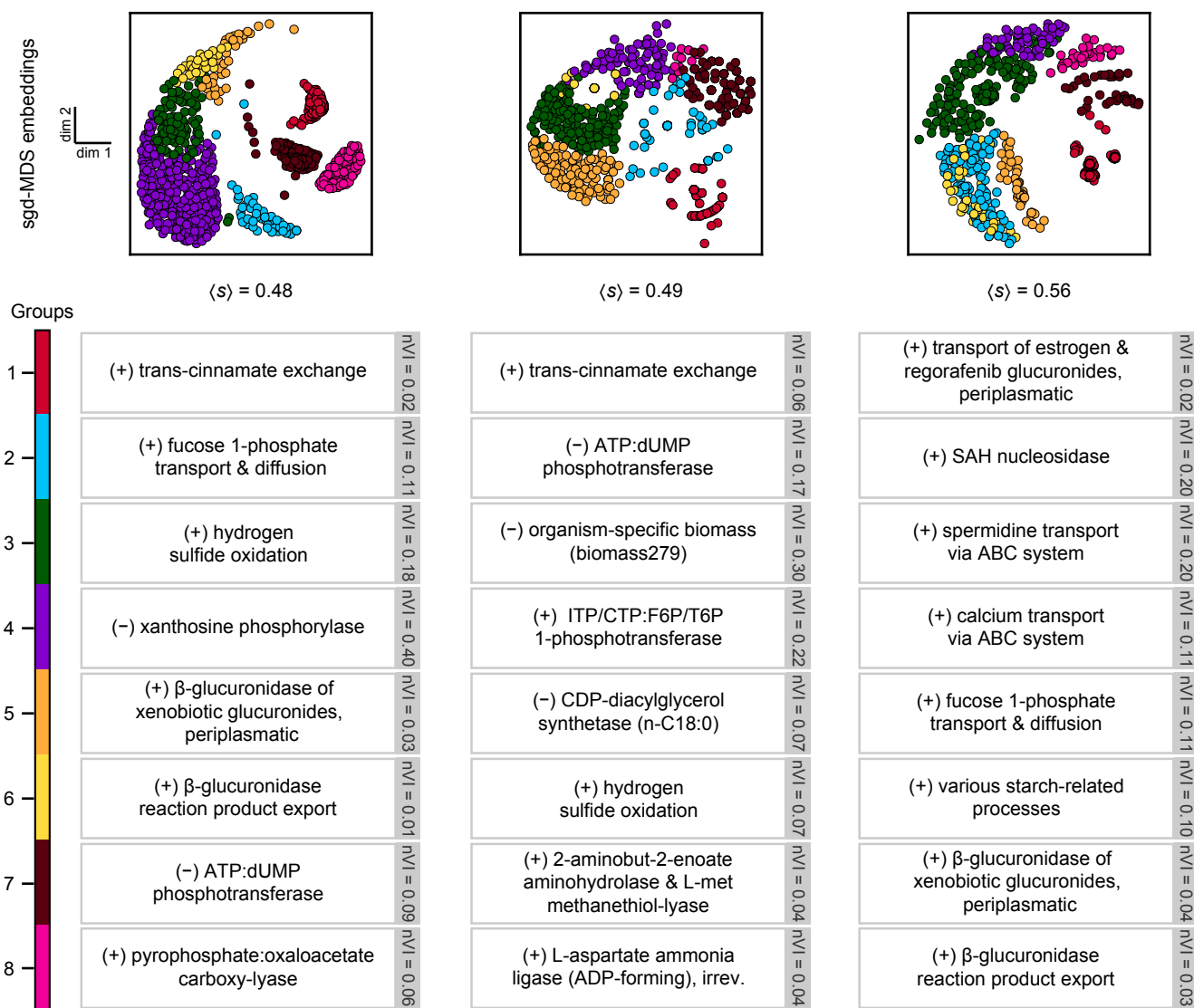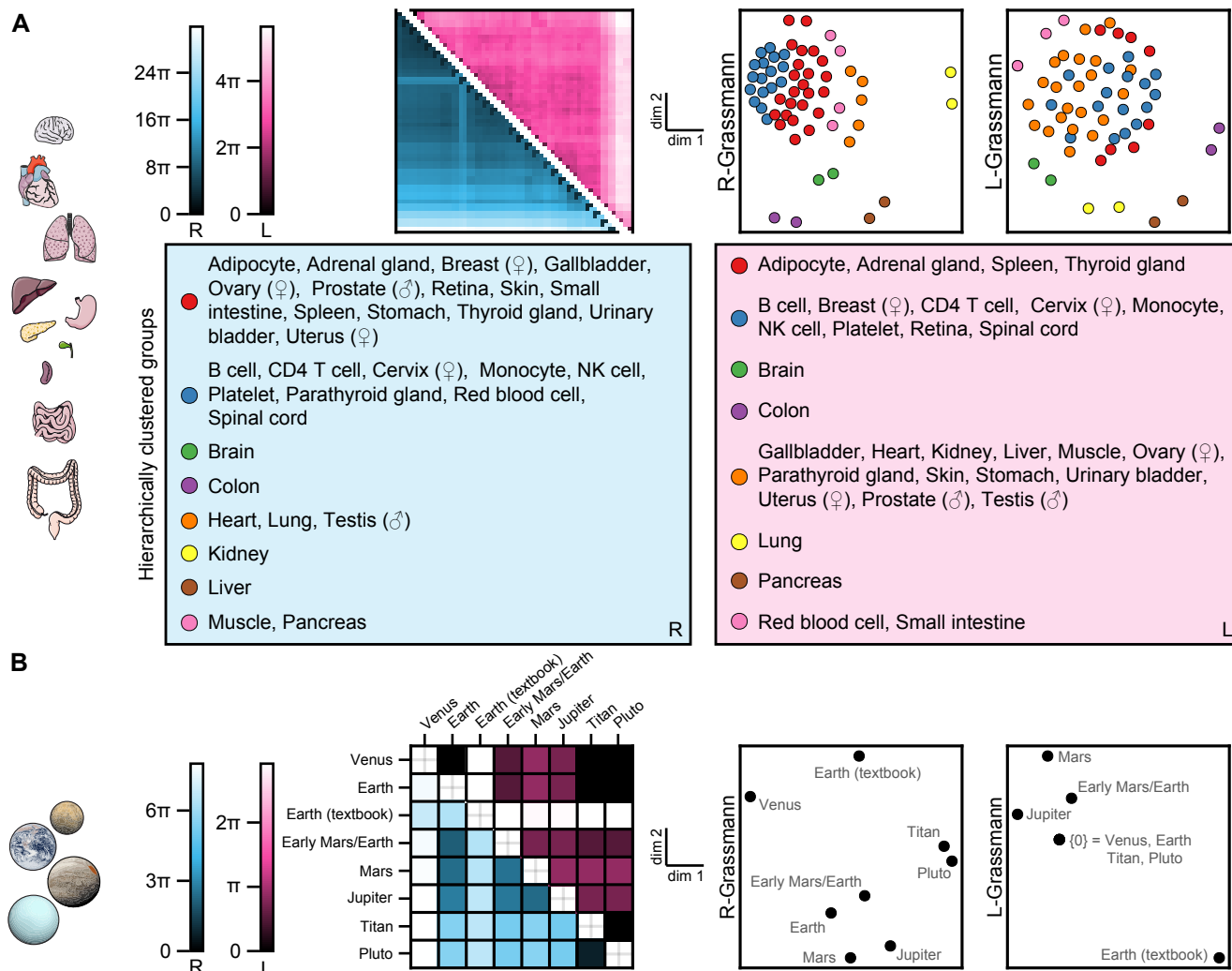
FIG. 5. **Hierarchical clustering of metabolic distances reveals functional groups of organisms enriched or depleted in specific metabolic processes.** Multidimensional scaling embeddings of the metabolic distance matrices are shown colored by clusters obtained by hierarchical clustering of the matrices with Ward linkage and a tree-cut to produce 8 disjoint clusters. We use normalized variation of information (nVI) to assess the validity of assignment to metabolic processes: zero nVI corresponds to perfect matching, whereas unity nVI corresponds to maximally distinct matching. Mean silhouette scores $\langle s \rangle$ are computed for each distance using the eight disjoint clusters as cluster assignments. Abbreviations: ABC = ATP-binding cassette transporters, ATP = adenosine triphosphate, CDP = cytosine diphosphate, CTP = cytosine triphosphate, F6P = fructose-6-phosphate, ITP = inosine triphosphate, SAH = S-adenosylhomocysteine, T6P = tagatose-6-phosphate, dUMP = deoxyuridine monophosphate.

network curatorial effects on Grassmann distances. We are aware that data on planetary chemical reaction networks are currently limited, but as more become available these can be incorporated.

DISCUSSION

Beyond optimal metabolic adaption

Experimental work has shown that deletion of the *pyk* gene in *E. coli* JM101 leads to local redistribution of metabolic reaction fluxes [70]. Subsequent *in silico* KOs of *E. coli* genome-scale metabolic reconstructions showed local redistributions of steady-state flux vectors obtained by minimization of metabolic adjust-

FIG. 6. **Comparisons of human tissues and planetary atmosphere highlights applicability of metabolic Grassmann distances to other complex chemical reaction networks.** (*A*) Multidimensional scaling embeddings of metabolic Grassmann distance computed on sex-specific human tissue and organ metabolic networks are shown colored by 8 clusters obtained by hierarchical clustering of the matrices with Ward linkage and a tree-cut to produce 8 disjoint clusters. The most distinct organs in the right nullspace are the kidneys, liver, colon, and brain, whereas for the left nullspace, we find that the pancreas, colon, lungs, and brain are distal. Graphical elements were adapted from Servier Medical Art under a Creative Commons Attribution 4.0 license. (*B*) Multidimensional scaling embeddings of Metabolic Grassmann distance computed on 8 published planetary atmosphere chemical reaction networks serve as a proof of concept based on limited data availability. As additional planetary networks becomes available, these can be incorporated. Distance matrix labels are in order of distance from the Sun. Human tissue and planetary atmosphere chemical reaction networks were obtained from [5] and [11], respectively. Planetary graphical elements were derived from photographs obtained from the National Aeronautics and Space Administration.

ment (MOMA). MOMA matches an element of the right nullspace in a genetically perturbed metabolic network to a flux balance analysis (FBA) solution of the wild-type (WT) metabolic network that minimizes the difference in fluxes, $\|v_{WT} - v_{KO}\|$, subject to additional flux constraints. MOMA fluxes are consistent with the hypothesis that laboratory KOs need not satisfy optimal metabolic adaptation [71]. Here we find a stronger statement: nearly all computationally viable gene KOs of *E. coli* K-12 MG1655 do not produce appreciable differences in the spaces of steady-state fluxes and conservation laws.

These results suggest that conservation laws and steady-state network fluxes critical for biological function are insulated from genetic perturbations. We note that this may aid in the design of synthetic organisms that recapitulate these salient metabolic features from wild nonsynthetic organisms [72–75]. Similarly, we should not be surprised if these principles are applicable to the search for Earth-like planetary atmospheres where specific steady-state fluxes and conservation laws may be critical for sustaining life.

Effects of network curation on metabolic distances

Any data-driven computational analysis is limited by data availability; chemical reaction networks are no different. In practice, genome-scale reconstructions of metabolism are limited by uncertainties present in the reconstruction pipeline such as incomplete or missing gene annotations [76]. The authors of AGORA2 [49] addressed these concerns using a semiautomated refinement pipeline that curatorially adds "missing" metabolic processes using experimental data and removes thermodynamically infeasible processes [14, 49]. Additionally, most of the planetary atmosphere networks examined here lack "textbook-level" detail—indicated by the distant textbook Earth network in Fig. 6B. Rather, these networks were constructed to reproduce known physical parameters and sparse chemical data [11]. Consequently, we caution against overinterpretations of distances between chemical reaction networks.

For the microbial networks considered here, the processes identified for R-Grassmann group 5 and Jaccard groups 1 & 7 occur across the periplasm, the region between the outer and inner cell membrane in bacteria with two membranes (diderms) or the region between the cell membrane and the cell well in bacteria with a single membrane (monoderms) [77–81]. In general, monoderms are Gram-positive and diderms are Gram-negative; however, there are notable exceptions [80, 81]. Previous work has shown that Gram stain reactivity of organisms produces well-defined clusters with the Jaccard distance [23]. We recapitulate this result with the Jaccard distance which outperforms the Grassmann distances in this regard (SI). We note that the Gram-negative networks in mini-AGORA2 have larger numbers of metabolic processes and metabolites than their Gram-positive counterparts (SI). Is it then surprising that the Jaccard distance, a metric based on set overlap and size, produces well-defined clusters on the basis of Gram-stain reactivity? We also note that AGORA2 networks were curated to include drug biotransformation and degradation reactions to enable the modeling of personalized gut microbial drug metabolism [49]. That we appreciably observe this feature when clustering with the R-Grassmann and Jaccard distances further underscores the need for a nuanced and context-aware interpretation of metabolic distances.

Open vs closed chemical reaction networks

Until now, we have considered open chemical reaction networks: systems forced away from thermodynamic equilibrium by the exchange of mass and energy with the environment. These exchanges are described by fluxes across the system boundary and correspond to columns of the stoichiometric matrix with all positive or negative entries (Fig. 1C). In open chemical reaction networks, the number of conservation laws observed cannot be larger than the number observed by their closed counterparts.

As such, while closed chemical reaction networks realize nontrivial left nullspaces, the does not always apply to about open networks [28, 38] (SI). Considering the form of the Grassmann distance metric (Eq. 2), L-Grassmann distances on closed networks will necessarily impose an upper bound on their open network counterparts. We notably observe this in the comparison of the planetary atmosphere networks, where four networks have a trivial left nullspace and consequently map to the same point in a sgd-MDS embedding (Fig. 6B). Consistent with an increase in the number of conservation laws, this degeneracy is remedied by the removal of exchange processes (SI). Although we also observe changes to the L-Grassmann distances of the microbial and human tissue networks (SI), we note that biological systems are phenomonologically open. Energetic and material demands for maintenance and growth are satisfied by the efflux of chemicals from the environment [28]. We do not address here the extent to which a chemical reaction network is open (or closed) at any given point in time. Instead, we take a conservative approach in using open networks as removing any exchange process with the environment may introduce additional conservation laws which are not guaranteed to hold for all time.

CONCLUSIONS

Recent experimental and computational developments provide us with the opportunity to develop functional classifications of chemical reaction networks grounded in physical principles. Here, we introduce a framework for the classification of these networks using differences between nullspaces of their stoichiometric matrices. In the human gut, this framework enables us to discover metabolic processes that describe groups of bacteria with similar steady-state fluxes and conservation laws. The generality of this framework, from chemical reaction networks in bacteria to human tissues to planetary atmospheres, can lead to the development of a universal atlas of chemical reaction networks in which systems across length scales must reside.

ACKNOWLEDGEMENTS

METHODS

Processing Chemical Reaction Networks

The bacterial networks were obtained from the AGORA2 dataset [49] (Fig. 1). We used the 688 out of the 7302 published metabolic networks which have complete comparative genomics [49]. The human tissue networks presented in this work were obtained from the Harvey and Harvetta reconstructions of human metabolism [5]. The planetary atmosphere networks were derived from [11] where chemicals without molecular formulas were removed and catalytic chemicals that appeared as both reactant and product were reduced to simplify stoichiometry. Any resulting processes without either reactants or products were taken to be exchange processes with the environment.

For each type of network, we sorted the columns and rows of the stoichiometric matrices alphabetically by chemical and metabolic process name, respectively using I/O functions implemented in the COBRA Toolbox v3.0 for Matlab (MathWorks) [82]. Correspondingly, any chemical and process not present in the network introduces a row or column of zeros accordingly. All information on biological metabolic processes and chemicals were obtained from the Virtual Metabolic Human (VMH) database and is presented here in its nomenclature [14].

Generating in silico knockouts

Genome-scale metabolic reconstructions, such as those in AGORA2, contain gene-protein-reaction (GPR) rules which are mapping from the presence of genes to the presence of metabolic processes. An *in silico* single gene knockout is obtained by evaluating these GPR rules with all other genes present and identifying which metabolic processes are as a result absent in the knockout. We assess network viability with flux balance analysis (FBA) and minimization of metabolic adjustment (MOMA) using methods available in the COBRA Toolbox [82] with Gurobi v11.0.2 [83]. A network is deemed to be viable *in silico* if it realizes a nonzero biomass flux in a flux distribution obtained from FBA or MOMA.

Flux and stoichiometric consistency

Without proper conditioning, any chemical reaction network may not be physically admissible. We ensure all networks considered here satisfy flux and stoichiometric consistency using methods available in the COBRA Toolbox [82, 84–87] with Gurobi v11.0.2 [83]. Flux consistency implies that each process of a chemical reaction network is active, realizing nonzero flux, in at least one flux distribution [84, 85, 87]. We remove flux inconsistent internal (non-exchange) processes to ensure we only consider active metabolic processes [85, 86]. Similarly,

reaction databases may contain stoichiometric inconsistencies [88], where the stoichiometry of processes is inconsistent with conservation of mass. To that end we identify and correct stoichiometric inconsistent internal processes [86].

Computing Phylogenetic Distance

Of these networks in mini-AGORA2, only one lacks an accessible genome link reported in [49]. As such, we neglect it from any analysis involving genetic content. To infer phylogenies from genome sequences, we take the approach used in [23] where the PhyloPhlAn pipeline [55] is applied to the available genome sequences as well as the genome sequence of the archaebacteria *Methanobrevibacter smithii* ATCC 35061. We root the resulting tree using *M. smithii* ATCC 35061 as the outgroup. We then compute pairwise tree distances and use the square root of these distances as this makes the resulting distance Euclidean-like [54]. Tree manipulations are performed using PhyloNetworks.jl [89].

Computing Metabolic Distances

As with the phylogenetic distances, we collect all pairwise metabolic distances in a distance matrix (Fig. 1) and proceed as follows for each metric.

To calculate the metabolic Grassmann distances, we compute basis vectors for the right nullspace using the SVD-based nullspace function from the LinearAlgebra.jl package in Julia, omitting columns and rows of zeros [35]. The left nullspace of a matrix M is obtained by calculating the right nullspace of the transposed matrix M^T. To keep all basis vectors across networks of the same dimension we enter zeros in indices that corresponding to those nonexistent processes and metabolites.

We then compute the Grassmann distance between two basis $A \in \mathrm{Gr}(k, \infty)$ and $B \in \mathrm{Gr}(\ell, \infty)$ using [29]:

$$d_{\mathrm{Gr}(\infty,\infty)}(A, B) = \left(|k - \ell|\, \pi^2/4 + \sum_{i=1}^{\min(k,\ell)} \theta_i^2 \right)^{1/2},$$

where the θ_i are the principal angles between the subspaces and are obtained from:

$$\Theta = \mathrm{diag}(\theta_1, \ldots, \theta_{\min(k,\ell)}) = \cos^{-1} \Sigma \quad \text{where} \quad A^\mathsf{T} B = U\Sigma V^\mathsf{T}.$$

For the Jaccard distance, we look at sets of chemical/transport processes and compute:

$$d_{\mathrm{J}}(S, T) = 1 - \#(S \cap T)/\#(S \cup T),$$

where $\#$ is the set cardinality function which counts the number of elements in the set.

Cluster Learning

We compute silhouette scores as goodness of clustering scores using the Julia Clustering.jl package [35, 90]. We identify clusters for metabolic distance matrix by hierarchical clustering with Ward linkage (Minimum Increase of Sum of Squares) and obtain clusters with a tree-cut to the desired level of granularity. To assign identities to clusters we perform a cluster comparison analysis for each cluster by masking assignments to inclusion within a cluster of interest and identifying which processes(s) are enriched or depleted in the cluster. Since certain processes are always jointly present in the networks, we group processes if they co-occur in the same manner across all our networks. We identify those processes that minimize the variation of information [59] between inclusion masked assignments and process presence.

For a set S, we consider binary partitions $X = \{X_1, X_2\}$ and $Y = \{Y_1, Y_2\}$, where the elements of a partition are disjoint subsets of S whose unions is S. VI is defined as [59]

$$\text{VI}(X, Y) = H(X) + H(Y) - 2I(X, Y)$$

where H is the entropy associated with clustering,

$$H(X) = -\sum_k P(k) \log P(k), \ \ P(k) = \frac{\#|X_k|}{\#|S|},$$

and I is the mutual information between clusterings,

$$I(X, Y) = \sum_{k,k'} P(k, k') \log \frac{P(k, k')}{P(k)P(k')},$$

$$P(k, k') = \frac{\#|X_k \cap Y_{k'}|}{\#|S|}.$$

For interpretability, we normalize VI by the maximally achievable value for binary partitions: $2 \log 2$. We perform clustering and cluster comparison analysis using the Julia Clustering.jl package [35].

Stochastic Gradient Descent Multidimensional Scaling

We embed distance matrices by stochastic gradient descent multidimenional scaling (sgd-MDS) with loss function

$$\mathcal{L}(u) = 2 \sum_{\langle i,j \rangle} w_{ij} (\text{dist}_{\mathcal{M}}(u_i, u_j) - d_{ij})^2$$

where $\text{dist}_{\mathcal{M}}$ is the distance function on the manifold $\mathcal{M}$ and $w_{ij} = d_{ij}^{-2}$ are the weights for each pair of points [91]. For Euclidean manifolds $\mathcal{M} = \mathbb{R}^n$, the distance function is the ℓ^2-norm. Taking a physical prescription, this loss function is equivalent to the Hamiltonian of a system of fully coupled springs with spring constants w_{ij} and equilibrium lengths d_{ij}. The optimization process is then a relaxation of the system to a minimum of the Hamiltonian as described in [92]. This is achieved by iterative gradient descent steps for each spring in a random permutation—with replacement—according to an exponentially decay annealing schedule $\eta(t) = e^{-\lambda t}$ of step sizes $\mu_{ij} = \eta w_{ij}$ for a fixed number of steps $t = 0 \rightarrow t_s - 1$ where $t_s = 1000$. The exponential decay rate is chosen to be $\lambda = (t_s - 1)^{-1} \log(\max w_{ij}/\varepsilon \min w_{ij})$, where $\varepsilon = 0.1$. To allow for convergence, this is followed by an annealing schedule of $\Theta(1/t)$ until the relative change in the loss function drops below a threshold $\delta = 10^{-8}$ or a fixed number of iterations $\tau_s = 1000$ are reached.

[1] D. McCloskey, B. Ø. Palsson, and A. M. Feist, Basic and applied uses of genome-scale metabolic network reconstructions of *Escherichia coli*, Molecular Systems Biology **9**, 661 (2013).

[2] M. Dal Bello, H. Lee, A. Goyal, and J. Gore, Resource-diversity relationships in bacterial communities reflect the network structure of microbial metabolism, Nature Ecology & Evolution **5**, 1424 (2021).

[3] G. Capovilla, R. Braakman, G. P. Fournier, T. Hackl, J. Schwartzman, X. Lu, A. Yelton, K. Longnecker, M. C. K. Soule, E. Thomas, G. Swarr, A. Mongera, J. G. Payette, K. G. Castro, J. R. Waldbauer, E. B. Kujawinski, O. X. Cordero, and S. W. Chisholm, Chitin utilization by marine picocyanobacteria and the evolution of a planktonic lifestyle, Proceedings of the National Academy of Sciences **120**, e2213271120 (2023).

[4] C. Jang, S. Hui, X. Zeng, A. J. Cowan, L. Wang, L. Chen, R. J. Morscher, J. Reyes, C. Frezza, H. Y. Hwang, A. Imai, Y. Saito, K. Okamoto, C. Vaspoli, L. Kasprenski, G. A. Zsido, J. H. Gorman, R. C. Gorman, and J. D. Rabinowitz, Metabolite Exchange between Mammalian Organs Quantified in Pigs, Cell Metabolism **30**, 594 (2019).

[5] I. Thiele, S. Sahoo, A. Heinken, J. Hertel, L. Heirendt, M. K. Aurich, and R. M. Fleming, Personalized whole-body models integrate metabolism, physiology, and the gut microbiome, Molecular Systems Biology **16**, e8982 (2020).

[6] H. J. Morowitz, The Derivation of Ecological Relationships from Physical and Chemical Principles, Proceedings of the National Academy of Sciences **71**, 2335 (1974).

[7] M. Feinberg and F. J. M. Horn, Dynamics of open chemical systems and the algebraic structure of the underlying reaction network, Chemical Engineering Science **29**, 775 (1974).

[8] T. Veloz and D. Flores, Reaction Network Modeling of Complex Ecological Interactions: Endosymbiosis and Multilevel Regulation, *Complexity*, Complexity **2021**, 8760937 (2021).

[9] M. Allen, Y. L. Yung, and J. W. Waters, Vertical transport and photochemistry in the terrestrial mesosphere and lower thermosphere (50–120 km), Journal of Geophysical Research: Space Physics **86**, 3617 (1981).

[10] R. V. Solé and A. Munteanu, The large-scale organization of chemical reaction networks in astrophysics, Europhysics Letters **68**, 170 (2004).

[11] M. L. Wong, A. Prabhu, J. Williams, S. M. Morrison, and R. M. Hazen, Toward Network-Based Planetary Biosignatures: Atmospheric Chemistry as Unipartite, Unweighted, Undirected Networks, Journal of Geophysical Research: Planets **128**, e2022JE007658 (2023).

[12] I. Thiele and B. Ø. Palsson, A protocol for generating a high-quality genome-scale metabolic reconstruction, Nature Protocols **5**, 93 (2010).

[13] L. Chen, W. Lu, L. Wang, X. Xing, Z. Chen, X. Teng, X. Zeng, A. D. Muscarella, Y. Shen, A. Cowan, M. R. McReynolds, B. J. Kennedy, A. M. Lato, S. R. Campagna, M. Singh, and J. D. Rabinowitz, Metabolite discovery through global annotation of untargeted metabolomics data, Nature Methods **18**, 1377 (2021).

[14] A. Heinken, S. Magnúsdóttir, R. M. T. Fleming, and I. Thiele, DEMETER: efficient simultaneous curation of genome-scale reconstructions guided by experimental data and refined gene annotations, Bioinformatics **37**, 3974 (2021).

[15] H. Qiang, F. Wang, W. Lu, X. Xing, H. Kim, S. A. Merette, L. B. Ayres, E. Oler, J. E. AbuSalim, A. Roichman, M. Neinast, R. A. Cordova, W. D. Lee, E. Herbst, V. Gupta, S. Neff, M. Hiebert-Giesbrecht, A. Young, V. Gautam, S. Tian, B. Wang, H. Röst, R. Greiner, L. Chen, C. W. Johnston, L. J. Foster, A. M. Shapiro, D. S. Wishart, J. D. Rabinowitz, and M. A. Skinnider, Language model-guided anticipation and discovery of unknown metabolites, bioRxiv 10.1101/2024.11.13.623458 (2024).

[16] J. Yang and R. Hu, Automated Chemical Reaction Network Generation and Its Application to Exoplanet Atmospheres, Astrophysical Journal **966**, 189 (2024).

[17] H. Jeckel, K. Nosho, K. Neuhaus, A. D. Hastewell, D. J. Skinner, D. Saha, N. Netter, N. Paczia, J. Dunkel, and K. Drescher, Simultaneous spatiotemporal transcriptomics and microscopy of Bacillus subtilis swarm development reveal cooperation across generations, Nature Microbiology **8**, 2378 (2023).

[18] X. Li, S. Hui, E. T. Mirek, W. O. Jonsson, T. G. Anthony, W. D. Lee, X. Zeng, C. Jang, and J. D. Rabinowitz, Circulating metabolite homeostasis achieved through mass action, Nature Metabolism **4**, 141 (2022).

[19] B. Yuan, W. Doxsey, Ö. Tok, Y.-Y. Kwon, Y. Liang, K. E. Inouye, G. S. Hotamışlıgil, and S. Hui, An organism-level quantitative flux model of energy metabolism in mice, Cell Metabolism 10.1016/j.cmet.2025.01.008 (2025).

[20] H. C. Vebø, M. Solheim, L. Snipen, I. F. Nes, and D. A. Brede, Comparative Genomic Analysis of Pathogenic and Probiotic *Enterococcus faecalis* Isolates, and Their Transcriptional Responses to Growth in Human Urine, PLOS ONE **5**, e12489 (2010).

[21] M. Arumugam, J. Raes, E. Pelletier, D. Le Paslier, T. Yamada, D. R. Mende, G. R. Fernandes, J. Tap, T. Bruls, J.-M. Batto, M. Bertalan, N. Borruel, F. Casellas, L. Fernandez, L. Gautier, T. Hansen, M. Hattori, T. Hayashi, M. Kleerebezem, K. Kurokawa, M. Leclerc, F. Levenez, C. Manichanh, H. B. Nielsen, T. Nielsen, N. Pons, J. Poulain, J. Qin, T. Sicheritz-Ponten, S. Tims, D. Torrents, E. Ugarte, E. G. Zoetendal, J. Wang, F. Guarner, O. Pedersen, W. M. de Vos, S. Brunak, J. Doré, M. Antolín, F. Artiguenave, H. Blottiere, M. Almeida, C. Brechot, C. Cara, C. Chervaux, A. Cultrone, C. Delorme, G. Denariaz, R. Dervyn, K. U. Foerstner, C. Friss, M. van de Guchte, E. Guedon, F. Haimet, W. Huber, J. van Hylckama-Vlieg, A. Jamet, C. Juste, G. Kaci, J. Knol, K. Kristiansen, O. Lakhdari, S. Layec, K. Le Roux, E. Maguin, A. Mérieux, R. Melo Minardi, C. M'rini, J. Muller, R. Oozeer, J. Parkhill, P. Renault, M. Rescigno, N. Sanchez, S. Sunagawa, A. Torrejon, K. Turner, G. Vandemeulebrouck, E. Varela, Y. Winogradsky, G. Zeller, J. Weissenbach, S. D. Ehrlich, P. Bork, and M. C. (additional members), Enterotypes of the human gut microbiome, Nature **473**, 174 (2011).

[22] J. M. Monk, P. Charusanti, R. K. Aziz, J. A. Lerman, N. Premyodhin, J. D. Orth, A. M. Feist, and B. Ø. Palsson, Genome-scale metabolic reconstructions of multiple *Escherichia coli* strains highlight strain-specific adaptations to nutritional environments, Proceedings of the National Academy of Sciences **110**, 20338 (2013).

[23] E. Bauer, C. C. Laczny, S. Magnusdottir, P. Wilmes, and I. Thiele, Phenotypic differentiation of gastrointestinal microbes is reflected in their encoded metabolic repertoires, Microbiome **3**, 55 (2015).

[24] G. Strang, The Fundamental Theorem of Linear Algebra, The American Mathematical Monthly **100**, 848 (1993).

[25] G. Strang, Introduction to Linear Algebra (Wellesley-Cambridge Press, Wellesley, MA, 2016) 5th ed.

[26] S. Schuster and C. Hilgetag, On Elementary Flux Mode in Biochemical Reaction Systems at Steady State, Journal of Biological Systems **2**, 165 (1994).

[27] C. H. Schilling, D. Letscher, and B. Ø. Palsson, Theory for the Systemic Definition of Metabolic Pathways and their use in Interpreting Metabolic Function from a Pathway-Oriented Perspective, Journal of Theoretical Biology **203**, 229 (2000).

[28] M. Polettini and M. Esposito, Irreversible thermodynamics of open chemical networks. I. Emergent cycles and broken conservation laws, The Journal of Chemical Physics **141**, 024117 (2014).

[29] K. Ye and L.-H. Lim, Schubert Varieties and Distances between Subspaces of Different Dimensions, SIAM Journal on Matrix Analysis and Applications **37**, 1176 (2016).

[30] S. Bi, M. Kargeti, R. Colin, N. Farke, H. Link, and V. Sourjik, Dynamic fluctuations in a bacterial metabolic network, Nature Communications **14**, 2173 (2023).

[31] M. Tantardini, F. Ieva, L. Tajoli, and C. Piccardi, Comparing methods for comparing networks, Scientific Reports **9**, 17557 (2019).

[32] P. Wills and F. G. Meyer, Metrics for graph comparison: A practitioner's guide, PLOS ONE **15**, e0228728 (2020).

[33] V. Mazumdar, S. Amar, and D. Segrè, Metabolic Proximity in the Order of Colonization of a Microbial Community, PLOS ONE **8**, e77617 (2013).

[34] J. Machicao, H. A. Filho, D. J. G. Lahr, M. Buckeridge, and O. M. Bruno, Topological assessment of metabolic networks reveals evolutionary information, Scientific Reports **8**, 15918 (2018).

[35] J. Bezanson, A. Edelman, S. Karpinski, and V. B. Shah, Julia: A Fresh Approach to Numerical Computing, SIAM

Review **59**, 65 (2017).

[36] A. Reuther, J. Kepner, C. Byun, S. Samsi, W. Arcand, D. Bestor, B. Bergeron, V. Gadepally, M. Houle, M. Hubbell, M. Jones, A. Klein, L. Milechin, J. Mullen, A. Prout, A. Rosa, C. Yee, and P. Michaleas, Interactive supercomputing on 40,000 cores for machine learning and data analysis, in *2018 IEEE HPEC* (IEEE, 2018) pp. 1–6.

[37] A. E. Motter, N. Gulbahce, E. Almaas, and A. Barabási, Predicting synthetic rescues in metabolic networks, *Molecular Systems Biology*, Molecular Systems Biology **4**, 168 (2008).

[38] I. Famili and B. Ø. Palsson, The convex basis of the left null space of the stoichiometric matrix leads to the definition of metabolically meaningful pools, Biophysical Journal **85**, 16 (2003).

[39] F. Avanzini, N. Freitas, and M. Esposito, Circuit Theory for Chemical Reaction Networks, Phys. Rev. X **13**, 021041 (2023).

[40] S. G. Marehalli Srinivas, F. Avanzini, and M. Esposito, Thermodynamics of Growth in Open Chemical Reaction Networks, Phys. Rev. Lett. **132**, 268001 (2024).

[41] S. G. Marehalli Srinivas, F. Avanzini, and M. Esposito, Characterizing the conditions for indefinite growth in open chemical reaction networks, Phys. Rev. E **109**, 064153 (2024).

[42] P. C. Maloney, E. R. Kashket, and T. H. Wilson, A protonmotive force drives atp synthesis in bacteria, Proceedings of the National Academy of Sciences **71**, 3896 (1974).

[43] N. R. Glasser, S. H. Saunders, and D. K. Newman, The colorful world of extracellular electron shuttles, Annual Review of Microbiology **71**, 731 (2017).

[44] R. D. Horak, J. A. Ciemniecki, and D. K. Newman, Bioenergetic suppression by redox-active metabolites promotes antibiotic tolerance in *Pseudomonas aeruginosa*, *Proceedings of the National Academy of Sciences*, Proceedings of the National Academy of Sciences **121**, e2406555121 (2024).

[45] N. Figueiredo, P. Georgieva, E. Lang, I. Santos, A. Teixeira, and A. Tomé, SSA of biomedical signals: A linear invariant systems approach, Statistics and Its Interface **3**, 345 (2010).

[46] E. Sharafuddin, N. Jiang, Y. Jin, and Z.-L. Zhang, Know Your Enemy, Know Yourself: Block-Level Network Behavior Profiling and Tracking, in *2010 IEEE Global Telecommunications Conference* (2010) pp. 1–6.

[47] A. E. Cohen, A. D. Hastewell, S. Pradhan, S. W. Flavell, and J. Dunkel, Schrödinger dynamics and berry phase of undulatory locomotion, Physical Review Letters **130**, 258402 (2023).

[48] P. Le Mercier, J. Bolleman, E. de Castro, E. Gasteiger, P. Bansal, A. H. Auchincloss, E. Boutet, L. Breuza, C. Casals-Casas, A. Estreicher, M. Feuermann, D. Lieberherr, C. Rivoire, I. Pedruzzi, N. Redaschi, and A. Bridge, Swissbiopics—an interactive library of cell images for the visualization of subcellular location data, Database **2022**, 10.1093/database/baac026 (2022).

[49] A. Heinken, J. Hertel, G. Acharya, D. A. Ravcheev, M. Nyga, O. E. Okpala, M. Hogan, S. Magnúsdóttir, F. Martinelli, B. Nap, G. Preciat, J. N. Edirisinghe, C. S. Henry, R. M. T. Fleming, and I. Thiele, Genome-scale metabolic reconstruction of 7,302 human microorganisms for personalized medicine, Nature Biotechnology **41**, 1320 (2023).

[50] C. Blanco, P. Ritzenthaler, and M. Mata-Gilsinger, Nucleotide sequence of a regulatory region of the *uidA* gene in *Escherichia coli* K12, Molecular and General Genetics MGG **199**, 101 (1985).

[51] G. Yang, S. Ge, R. Singh, S. Basu, K. Shatzer, M. Zen, J. Liu, Y. Tu, C. Zhang, J. Wei, J. Shi, L. Zhu, Z. Liu, Y. Wang, S. Gao, and M. Hu, Glucuronidation: driving factors and their impact on glucuronide disposition, Drug Metabolism Reviews **49**, 105 (2017).

[52] S. Gao, R. Sun, R. Singh, S. Yu So, C. T. Chan, T. Savidge, and M. Hu, The role of gut microbial β-glucuronidase in drug disposition and development, Drug Discovery Today **27**, 103316 (2022).

[53] M. T. Martins, I. G. Rivera, D. L. Clark, M. H. Stewart, R. L. Wolfe, and B. H. Olson, Distribution of *uidA* gene sequences in *Escherichia coli* isolates in water sources and comparison with the expression of β-glucuronidase activity in 4-methylumbelliferyl-beta-D-glucuronide media, Applied and Environmental Microbiology **59**, 2271 (1993).

[54] D. M. de Vienne, G. Aguileta, and S. Ollier, Euclidean Nature of Phylogenetic Distance Matrices, Systematic Biology **60**, 826 (2011).

[55] F. Asnicar, A. M. Thomas, F. Beghini, C. Mengoni, S. Manara, P. Manghi, Q. Zhu, M. Bolzan, F. Cumbo, U. May, J. G. Sanders, M. Zolfo, E. Kopylova, E. Pasolli, R. Knight, S. Mirarab, C. Huttenhower, and N. Segata, Precise phylogenetic analysis of microbial isolates and genomes from metagenomes using PhyloPhlAn 3.0, Nature Communications **11**, 2500 (2020).

[56] J. R. Zaneveld, C. Lozupone, J. I. Gordon, and R. Knight, Ribosomal RNA diversity predicts genome diversity in gut bacteria and their relatives, Nucleic Acids Research **38**, 3869 (2010).

[57] J. Felsenstein, *Inferring Phylogenies* (Sinauer Associates, Inc., Sunderland, MA, 2004).

[58] F. Delsuc, H. Brinkmann, and H. Philippe, Phylogenomics and the reconstruction of the tree of life, Nature Reviews Genetics **6**, 361 (2005).

[59] M. Meilă, Comparing Clusterings by the Variation of Information, in *Learning Theory and Kernel Machines*, edited by B. Schölkopf and M. K. Warmuth (Springer Berlin Heidelberg, Berlin, Heidelberg, 2003) pp. 173–187.

[60] J. M. Berg, T. J. L., G. J. Gatto, Jr., and S. Lubert, *Biochemistry*, 8th ed. (W. H. Freeman & Company, New York, NY, 2015).

[61] Y. Chiba, R. Kamikawa, K. Nakada-Tsukui, Y. Saito-Nakano, and T. Nozaki, Discovery of PP$_i$-type Phosphoenolpyruvate Carboxykinase Genes in Eukaryotes and Bacteria, Journal of Biological Chemistry **290**, 23960 (2015).

[62] J. G. Koendjbiharie, R. van Kranenburg, and S. W. M. Kengen, The PEP-pyruvate-oxaloacetate node: variation at the heart of metabolism, FEMS Microbiology Reviews **45**, fuaa061 (2020).

[63] N. J. Blunsom and S. Cockcroft, CDP-Diacylglycerol Synthases (CDS): Gateway to Phosphatidylinositol and Cardiolipin Synthesis, Frontiers in Cell and Developmental Biology **8**, 10.3389/fcell.2020.00063 (2020).

[64] L. L. Barton, N. L. Ritz, G. D. Fauque, and H. C. Lin, Sulfur Cycling and the Intestinal Microbiome, Digestive Diseases and Sciences **62**, 2241 (2017).

[65] S. J. Wolfson, R. Hitchings, K. Peregrina, Z. Cohen, S. Khan, T. Yilmaz, M. Malena, E. D. Goluch, L. Au-

genlicht, and L. Kelly, Bacterial hydrogen sulfide drives cryptic redox chemistry in gut microbial communities, Nature Metabolism **4**, 1260 (2022).

[66] J. M. Ravel, S. Norton, J. S. Humphreys, and W. Shive, Asparagine Biosynthesis in *Lactobacillus arabinosus* and Its Control by Asparagine through Enzyme Inhibition and Repression, Journal of Biological Chemistry **237**, 2845 (1962).

[67] M. P. Thomas and B. V. Potter, The structural biology of oestrogen metabolism, The Journal of Steroid Biochemistry and Molecular Biology **137**, 27 (2013).

[68] A. L. Davidson and J. Chen, ATP-Binding Cassette Transporters in Bacteria, Annual Review of Biochemistry **73**, 241 (2004).

[69] I. L. Weissman, D. J. Anderson, and F. Gage, Stem and Progenitor Cells: Origins, Phenotypes, Lineage Commitments, and Transdifferentiations, Annual Review of Cell and Developmental Biology **17**, 387 (2001).

[70] M. Emmerling, M. Dauner, A. Ponti, J. Fiaux, M. Hochuli, T. Szyperski, K. Wüthrich, J. E. Bailey, and U. Sauer, Metabolic Flux Responses to Pyruvate Kinase Knockout in *Escherichia coli*, Journal of Bacteriology **184**, 152 (2002).

[71] D. Segrè, D. Vitkup, and G. M. Church, Analysis of optimality in natural and perturbed metabolic networks, Proceedings of the National Academy of Sciences **99**, 15112 (2002).

[72] B. J. Yu, B. H. Sung, M. D. Koob, C. H. Lee, J. H. Lee, W. S. Lee, M. S. Kim, and S. C. Kim, Minimization of the *Escherichia coli* genome using a Tn5-targeted Cre/loxP excision system, Nature Biotechnology **20**, 1018 (2002).

[73] O. Aydin, A. P. Passaro, R. Raman, S. E. Spellicy, R. P. Weinberg, R. D. Kamm, M. Sample, G. A. Truskey, J. Zartman, R. D. Dar, S. Palacios, J. Wang, J. Tordoff, N. Montserrat, R. Bashir, M. T. A. Saif, and R. Weiss, Principles for the design of multicellular engineered living systems, APL Bioengineering **6**, 010903 (2022).

[74] R. Z. Moger-Reischer, J. I. Glass, K. S. Wise, L. Sun, D. M. C. Bittencourt, B. K. Lehmkuhl, D. R. Schoolmaster, M. Lynch, and J. T. Lennon, Evolution of a minimal cell, Nature **620**, 122 (2023).

[75] M. S. Y. Mardoukhi, J. Rapp, I. Irisarri, K. Gunka, H. Link, J. Marienhagen, J. de Vries, J. Stülke, and F. M. Commichau, Metabolic rewiring enables ammonium assimilation via a non-canonical fumarate-based pathway, *Microbial Biotechnology*, Microbial Biotechnology **17**, e14429 (2024).

[76] D. B. Bernstein, S. Sulheim, E. Almaas, and D. Segrè, Addressing uncertainty in genome-scale metabolic model reconstruction and analysis, Genome Biology **22**, 64 (2021).

[77] J. A. Hobot, E. Carlemalm, W. Villiger, and E. Kellenberger, Periplasmic gel: new concept resulting from the reinvestigation of bacterial cell envelope ultrastructure by new methods, Journal of Bacteriology **160**, 143 (1984).

[78] R. S. Gupta, What are archaebacteria: life's third domain or monoderm prokaryotes related to Gram-positive bacteria? A new proposal for the classification of prokaryotic organisms, Molecular Microbiology **29**, 695 (1998).

[79] V. R. F. Matias and T. J. Beveridge, Cryo-electron microscopy reveals native polymeric cell wall structure in *Bacillus subtilis* 168 and the existence of a periplasmic space, Molecular Microbiology **56**, 240 (2005).

[80] I. C. Sutcliffe, A phylum level perspective on bacterial cell envelope architecture, Trends in Microbiology **18**, 464 (2010).

[81] E. I. Tocheva, D. R. Ortega, and G. J. Jensen, Sporulation, bacterial cell envelopes and the origin of life, Nature Reviews Microbiology **14**, 535 (2016).

[82] L. Heirendt, S. Arreckx, T. Pfau, S. N. Mendoza, A. Richelle, A. Heinken, H. S. Haraldsdóttir, J. Wachowiak, S. M. Keating, V. Vlasov, S. Magnusdóttir, C. Y. Ng, G. Preciat, A. Žagare, S. H. J. Chan, M. K. Aurich, C. M. Clancy, J. Modamio, J. T. Sauls, A. Noronha, A. Bordbar, B. Cousins, D. C. El Assal, L. V. Valcarcel, I. Apaolaza, S. Ghaderi, M. Ahookhosh, M. Ben Guebila, A. Kostromins, N. Sompairac, H. M. Le, D. Ma, Y. Sun, L. Wang, J. T. Yurkovich, M. A. P. Oliveira, P. T. Vuong, L. P. El Assal, I. Kuperstein, A. Zinovyev, H. S. Hinton, W. A. Bryant, F. J. Aragón Artacho, F. J. Planes, E. Stalidzans, A. Maass, S. Vempala, M. Hucka, M. A. Saunders, C. D. Maranas, N. E. Lewis, T. Sauter, B. Ø. Palsson, I. Thiele, and R. M. T. Fleming, Creation and analysis of biochemical constraint-based models using the COBRA Toolbox v.3.0, Nature Protocols **14**, 639 (2019).

[83] Gurobi Optimization, LLC, Gurobi Optimizer Reference Manual (2024).

[84] V. Acuña, F. Chierichetti, V. Lacroix, A. Marchetti-Spaccamela, M.-F. Sagot, and L. Stougie, Modes and cuts in metabolic networks: Complexity and algorithms, Biosystems **95**, 51 (2009).

[85] N. Vlassis, M. P. Pacheco, and T. Sauter, Fast Reconstruction of Compact Context-Specific Metabolic Network Models, PLOS Computational Biology **10**, e1003424 (2014).

[86] I. Thiele, N. Vlassis, and R. M. T. Fleming, fastGapFill: efficient gap filling in metabolic networks, Bioinformatics **30**, 2529 (2014).

[87] R. M. T. Fleming, H. S. Haraldsdottir, L. H. Minh, P. T. Vuong, T. Hankemeier, and I. Thiele, Cardinality optimization in constraint-based modelling: application to human metabolism, Bioinformatics **39**, btad450 (2023).

[88] A. Gevorgyan, M. G. Poolman, and D. A. Fell, Detection of stoichiometric inconsistencies in biomolecular models, Bioinformatics **24**, 2245 (2008).

[89] C. Solís-Lemus, P. Bastide, and C. Ané, PhyloNetworks: A Package for Phylogenetic Networks, Molecular Biology and Evolution **34**, 3292 (2017).

[90] P. J. Rousseeuw, Silhouettes: A graphical aid to the interpretation and validation of cluster analysis, Journal of Computational and Applied Mathematics **20**, 53 (1987).

[91] W. S. Torgerson, Multidimensional scaling: I. Theory and method, Psychometrika **17**, 401 (1952).

[92] J. X. Zheng, S. Pawar, and D. F. M. Goodman, Graph Drawing by Stochastic Gradient Descent, IEEE Transactions on Visualization and Computer Graphics **25**, 2738 (2019).

Supplemental Materials: Functional classification of metabolic networks

I.   THE SQUARE ROOT OF A METRIC IS A METRIC

We take the square root of the tree graph metric as a definition of phylogenetic distance. We prove here that this distance is a metric by showing that, more generally, the square root ($\sqrt{} : \mathbb{R}_{\geq 0} \to \mathbb{R}_{\geq 0}$) of any metric is a metric. Suppose that we have a metric d that, by definition, satisfies the axioms:

1. $d(x, x) = 0$,

2. $x \neq y \implies d(x, y) > 0$,

3. $d(x, y) = d(y, x)$, and

4. $d(x, z) \leq d(x, y) + d(y, z)$.

Then the metric $\tilde{d} \equiv \sqrt{d}$ is also a metric:

1. $\tilde{d}(x, x) = \sqrt{d(x, x)} = 0$,

2. $x \neq y \implies \tilde{d}(x, y) = \sqrt{d(x, y)} > 0$,

3. $\tilde{d}(x, y) = \sqrt{d(x, y)} = \sqrt{d(y, x)} = \tilde{d}(y, x)$, and

4.

$$\tilde{d}(x, y) = \sqrt{d(x, z)} \leq \sqrt{d(x, y) + d(y, z)} \leq \sqrt{d(x, y) + d(y, z) + 2\sqrt{d(x, y)d(y, z)}}$$
$$= \sqrt{\left(\sqrt{d(x, y)} + \sqrt{d(y, z)}\right)^2} = \sqrt{d(x, y)} + \sqrt{d(y, z)} = \tilde{d}(x, y) + \tilde{d}(y, z).$$

■

II.   BROKEN CONSERVATION LAWS

Consider the simple three-component (A, B, C) closed chemical reaction network [S38] with stoichiometric matrix

$$S_{\text{int}} = \begin{bmatrix} -1 \\ -1 \\ 1 \end{bmatrix},$$

and corresponding nullspaces,

$$\mathcal{N}^{\text{R}}(S_{\text{int}}) = 0 \quad \text{and} \quad \mathcal{N}^{\text{L}}(S_{\text{int}}) = \begin{bmatrix} -1/\sqrt{6} & 1/\sqrt{2} \\ 2/\sqrt{6} & 0 \\ 1/\sqrt{6} & 1/\sqrt{2} \end{bmatrix}.$$

Note that the right nullspace only consists of the trivial zero vector. The left nullspace provides two conservation laws for the three components:

$$[A] + [C] = \text{const and}$$
$$[B] + [C] = \text{const.}$$

If we open the system by allowing exchange of the three components with the environment, the stoichiometric matrix becomes

$$S_{\text{exch}} = \begin{bmatrix} -1 & 1 & 0 & 0 \\ -1 & 0 & 1 & 0 \\ 1 & 0 & 0 & -1 \end{bmatrix}$$

where we now obtain a trivial left nullspace and a nontrivial right nullspace:

$$\mathcal{N}^{\mathrm{R}}(S_{\mathrm{exch}}) = \begin{bmatrix} 1/2 \\ 1/2 \\ 1/2 \\ 1/2 \end{bmatrix} \quad \text{and} \quad \mathcal{N}^{\mathrm{L}}(S_{\mathrm{exch}}) = 0.$$

The nontrivial right nullspace provides that at steady state the fluxes are all equivalent:

$$v_{\mathrm{reaction}} = v_{A\,\mathrm{influx}} = v_{B\,\mathrm{influx}} = v_{C\,\mathrm{efflux}}.$$

Re-closing the system by introducing three analogous chemical species in the environment provides the augmented stoichiometric matrix

$$S_{\mathrm{tot}} = \begin{bmatrix} -1 & 1 & 0 & 0 \\ -1 & 0 & 1 & 0 \\ 1 & 0 & 0 & -1 \\ 0 & -1 & 0 & 0 \\ 0 & 0 & -1 & 0 \\ 0 & 0 & 0 & 1 \end{bmatrix},$$

where we again obtain a trivial right nullspace and nontrivial left nullspace:

$$\mathcal{N}^{\mathrm{R}}(S_{\mathrm{tot}}) = 0 \quad \text{and} \quad \mathcal{N}^{\mathrm{L}}(S_{\mathrm{tot}}) = \begin{bmatrix} -1/2\sqrt{3} & 1/2 \\ 1/\sqrt{3} & 0 \\ 1/2\sqrt{3} & 1/2 \\ -1/2\sqrt{3} & 1/2 \\ 1/\sqrt{3} & 0 \\ 1/2\sqrt{3} & 1/2 \end{bmatrix}.$$

The corresponding conservation laws are

$$[A]_{\mathrm{tot}} + [C]_{\mathrm{tot}} = \mathrm{const} \text{ and}$$
$$[B]_{\mathrm{tot}} + [C]_{\mathrm{tot}} = \mathrm{const},$$

where $[X]_{\mathrm{tot}} = [X] + [X]_{\mathrm{ext}}$ for $X \in \{A, B, C\}$.

A

B

C
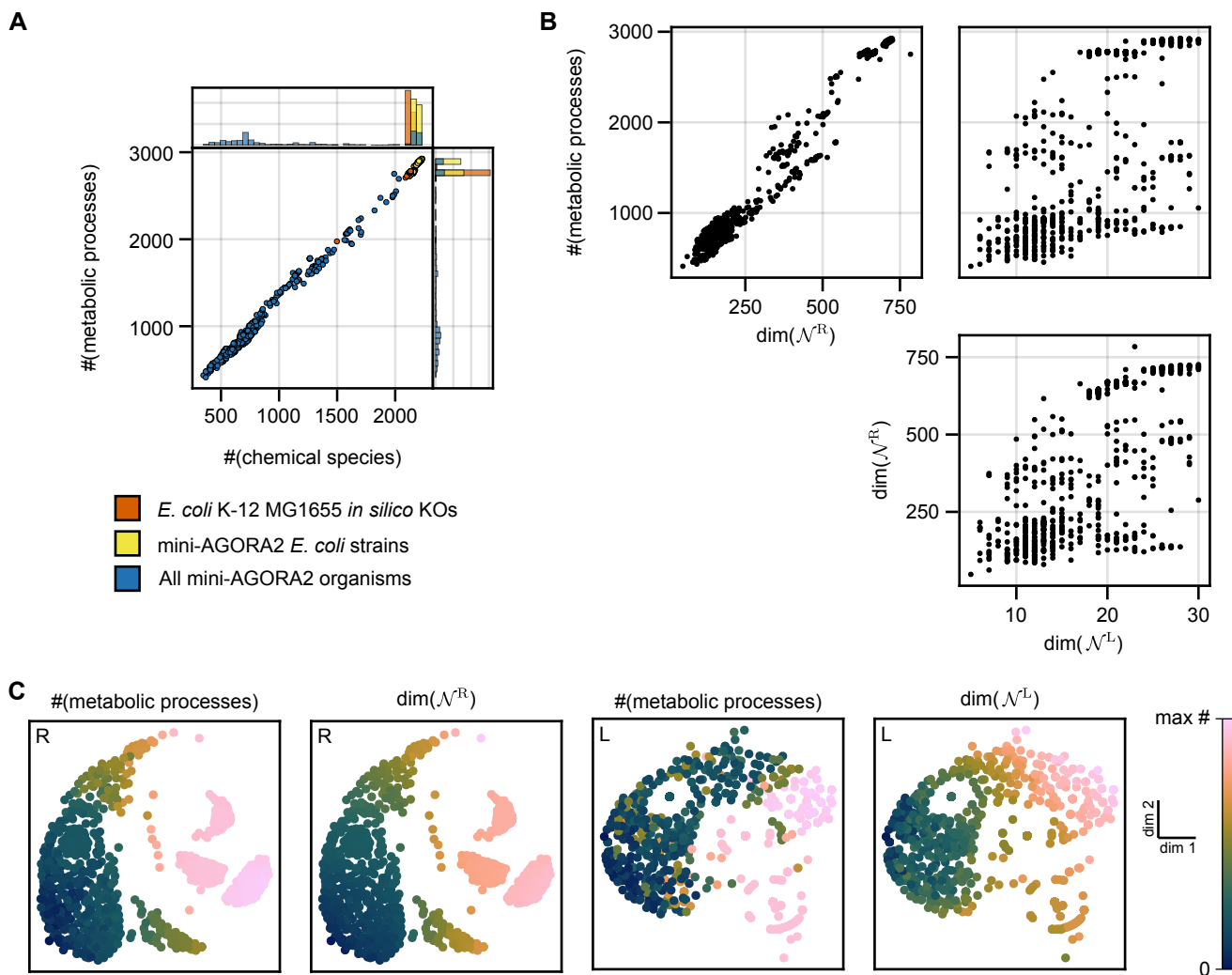
FIG. S1. **Dimension of right nullspace colors direction in R-Grassmann embedding.** Bacterial network size (A) is linearly predictive of the right nullspace dimension, in contrast to the left nullspace (B). (C) Colorings the sgd-MDS embedding of the R-Grassmann distance matrix by network size and nullspace dimension are consistent with directions corresponding to nullspace size.
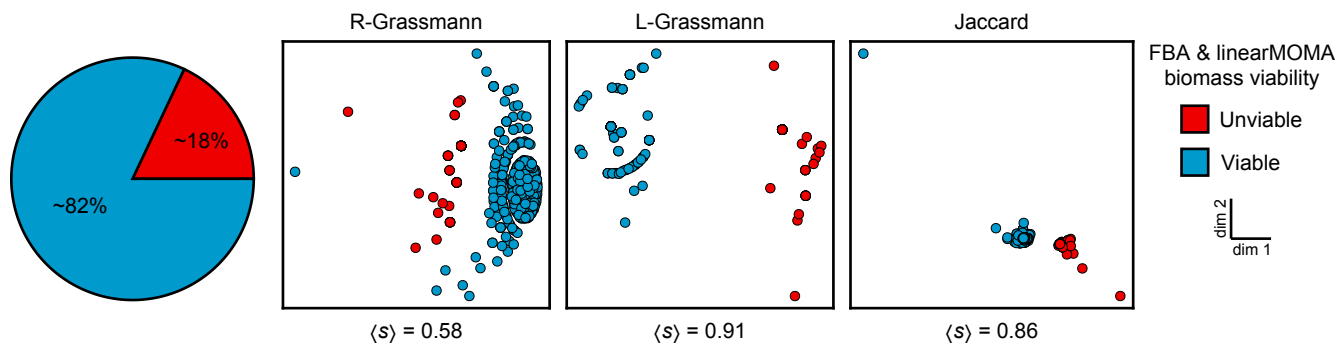
FIG. S2. *in silico E. coli* **KO viability is readily identified by the L-Grassmann distance.** Viability *E. coli* KOs is assessed by flux balance analysis (FBA) and minimization of metabolic adjustment (MOMA). A network is viable if it realizes a nonzero biomass flux in any flux distribution. We observe no differences in viability arising from the choice of FBA versus MOMA. Mean silhouette scores of the *E. coli* distance matrix, with viability as cluster assignment, reveals that the L-Grassmann distance captures differences in KO viability.
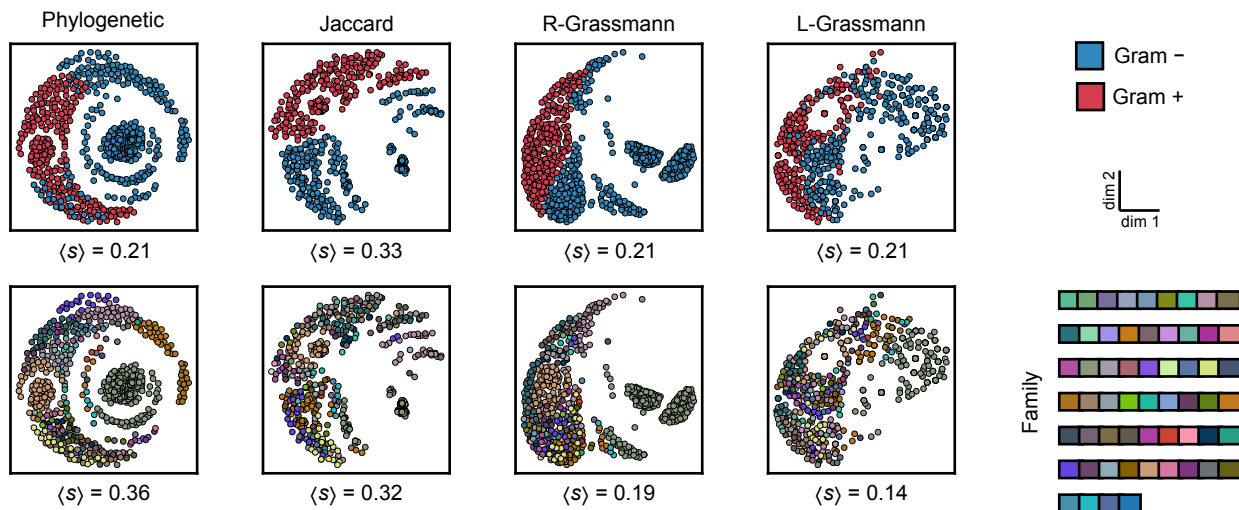
FIG. S3. **Biology-informed cluster assignments lead to metric-specific differences in cluster quality.** Two dimensional embeddings of genetic and metabolic distance matrices are coloring by gram stain reactivity (*Top*) and bacterial family (*Bottom*). Clusters quality using Gram stain reactivity as cluster assignment is largest for the Jaccard distance, but largest for the phylogenetic distance when using bacterial family, a genetic classification, as cluster assignments. This further suggests that metabolic Grassmann distances go beyond recapitulating genetic variation. Cluster quality is measured by the mean silhouette score.

R-Grassmann | L-Grassmann | Jaccard

Hierarchical groups

nVI: 0.40 — 0.00

R-Grassmann: A B / I III IV II / 1 4 7 8 3 2 5 6

L-Grassmann: A B / I III II IV / 1 3 2 5 4 8 7

Jaccard: A B / I III II IV / 1 7 3 2 4 5 6 8

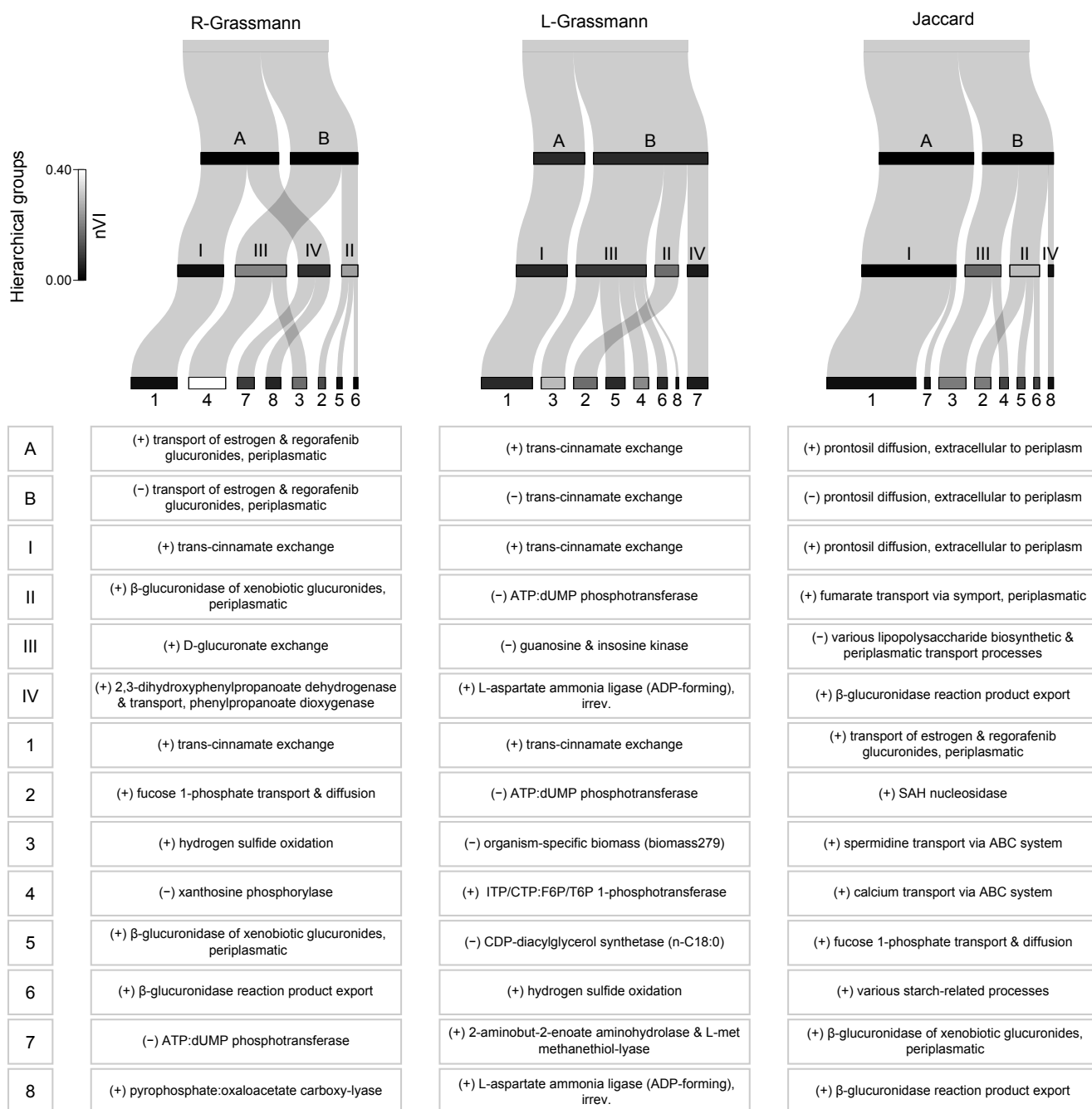|	R-Grassmann	L-Grassmann	Jaccard
A	(+) transport of estrogen & regorafenib glucuronides, periplasmatic	(+) trans-cinnamate exchange	(+) prontosil diffusion, extracellular to periplasm
B	(−) transport of estrogen & regorafenib glucuronides, periplasmatic	(−) trans-cinnamate exchange	(−) prontosil diffusion, extracellular to periplasm
I	(+) trans-cinnamate exchange	(+) trans-cinnamate exchange	(+) prontosil diffusion, extracellular to periplasm
II	(+) β-glucuronidase of xenobiotic glucuronides, periplasmatic	(−) ATP:dUMP phosphotransferase	(+) fumarate transport via symport, periplasmatic
III	(+) D-glucuronate exchange	(−) guanosine & insosine kinase	(−) various lipopolysaccharide biosynthetic & periplasmatic transport processes
IV	(+) 2,3-dihydroxyphenylpropanoate dehydrogenase & transport, phenylpropanoate dioxygenase	(+) L-aspartate ammonia ligase (ADP-forming), irrev.	(+) β-glucuronidase reaction product export
1	(+) trans-cinnamate exchange	(+) trans-cinnamate exchange	(+) transport of estrogen & regorafenib glucuronides, periplasmatic
2	(+) fucose 1-phosphate transport & diffusion	(−) ATP:dUMP phosphotransferase	(+) SAH nucleosidase
3	(+) hydrogen sulfide oxidation	(−) organism-specific biomass (biomass279)	(+) spermidine transport via ABC system
4	(−) xanthosine phosphorylase	(+) ITP/CTP:F6P/T6P 1-phosphotransferase	(+) calcium transport via ABC system
5	(+) β-glucuronidase of xenobiotic glucuronides, periplasmatic	(−) CDP-diacylglycerol synthetase (n-C18:0)	(+) fucose 1-phosphate transport & diffusion
6	(+) β-glucuronidase reaction product export	(+) hydrogen sulfide oxidation	(+) various starch-related processes
7	(−) ATP:dUMP phosphotransferase	(+) 2-aminobut-2-enoate aminohydrolase & L-met methanethiol-lyase	(+) β-glucuronidase of xenobiotic glucuronides, periplasmatic
8	(+) pyrophosphate:oxaloacetate carboxy-lyase	(+) L-aspartate ammonia ligase (ADP-forming), irrev.	(+) β-glucuronidase reaction product export

FIG. S4. **Effects of granularity on learning functional metabolic groups.** In the spirit of phylogenetic taxonomy, we hierarchical cluster metabolic distances into 2, 4, and 8 groups using Ward's linkage. River diagrams show the persistence and splitting of networks in each metabolic group. Correspondingly, the metabolic processes attributed to each group either persist or change demonstrating that, much like classifications in phylogenetic taxonomies, an *a priori* choice of granularity can affect learned functional differences. Box color and line thickness corresponds to normalized variation of information and number of networks, respectively.
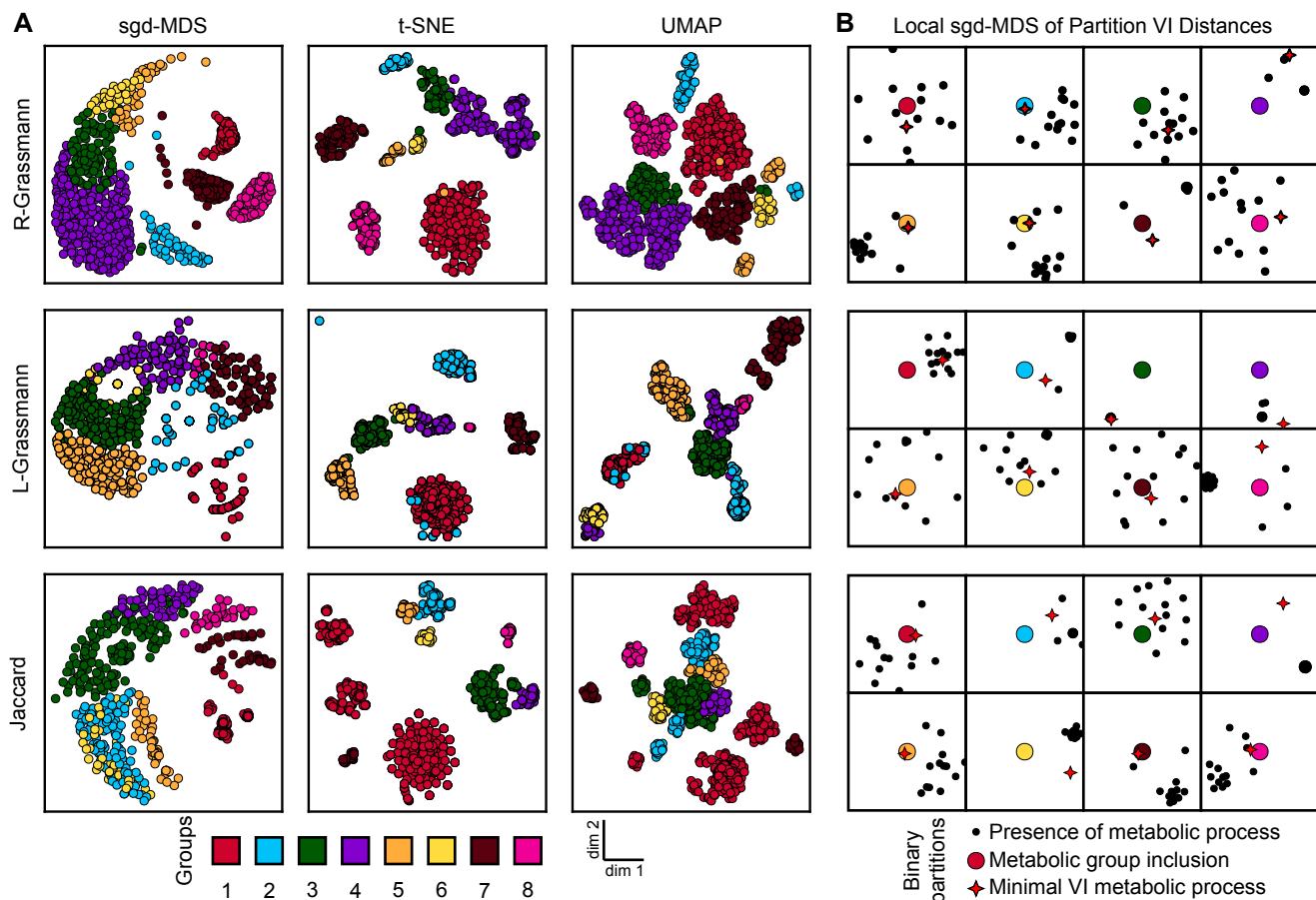
FIG. S5. **Embeddings of distances highlight that metabolic groups are robust to the choice of embedding procedure.** (*A*) Colors correspond to metabolic groups identifies in Fig. 5. t-SNE complexity and learning rate are set to 25 and 50, respectively. UMAP # neighbors and minimum distance are set to 10 and 2, respectively. (*B*) For each partition based on metabolic group inclusion, we perform a local sgd-MDS embeddings against the 19 nearest partitions based on the presence of metabolic processes. These embeddings demonstrate the local binary partition structure of the identified metabolic groups. Local sgd-MDS parameters: $\varepsilon = 0.1$, $t_s = 10,000$, $\tau_s = 10,000$, $\delta = 10^{-8}$.
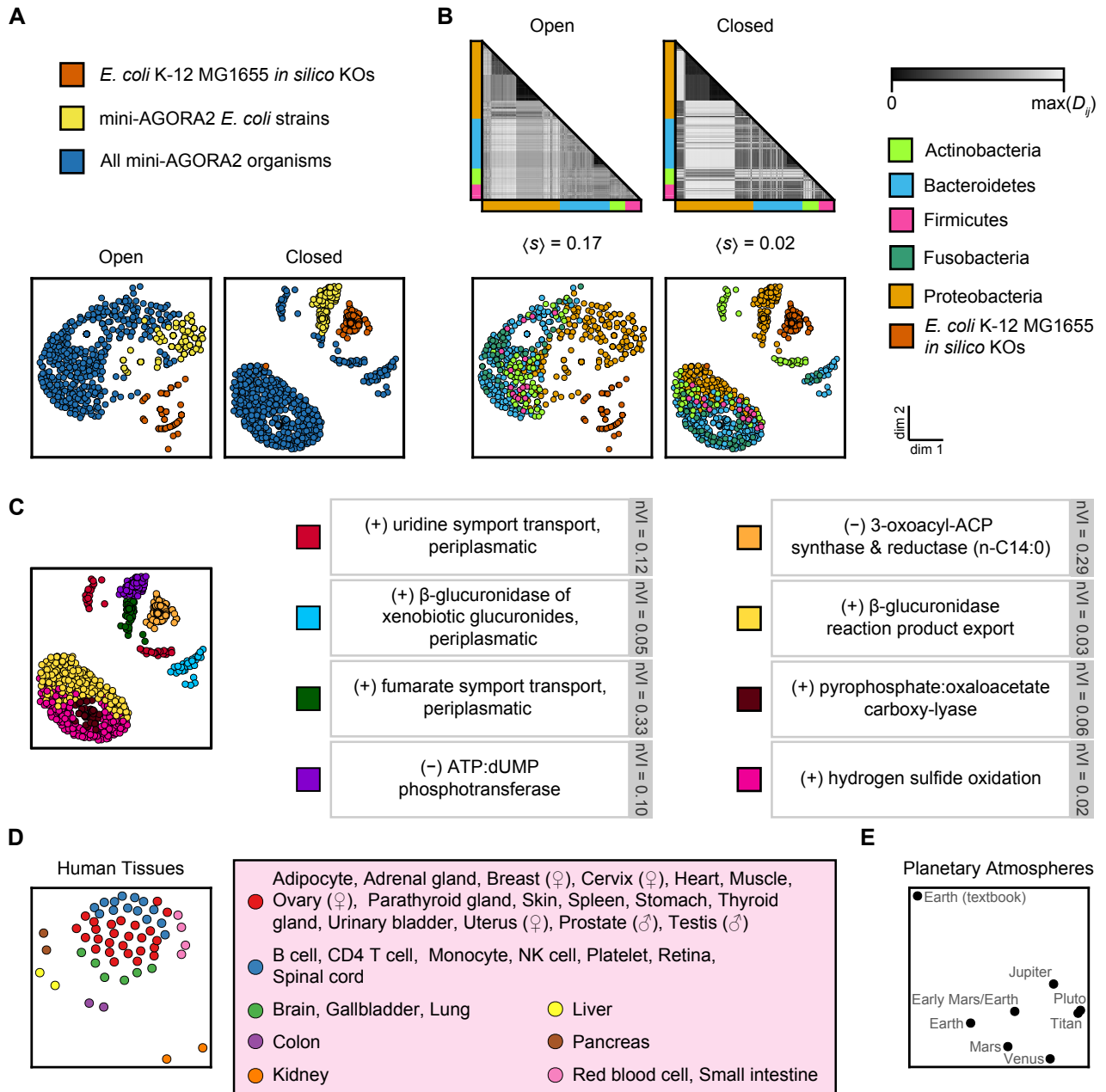
FIG. S6. **Closing open chemical reaction network leads to changes in conservation laws.** (*A*) sgd-MDS embeddings of closed bacterial metabolic networks show improved separation of non-*E. coli* networks from *E. coli* networks. (*B*) Conservation laws in closed bacterial metabolic network demonstrate the same loss of adherence to phylogenetic categories as their open counterparts. (*C*) Our cluster comparison analysis on the L-Grassmann distance of closed bacterial metabolic networks leads to the identification of metabolic processes previously identified by the R-Grassmann distance of open counterparts. Conservation laws in human tissues (*D*) and planetary atmospheres (*E*) are also affected by network closure. Abbreviations: ACP = acyl carrier protein, ATP = adenosine triphosphate, dUMP = deoxyuridine monophosphate.